INL/RPT-22-66720
Revision 0

Initial Observations from Advanced Gas Reactor (AGR)-5/6/7 Capsule 1

April 2022

John D. Stempien, Joe J. Palmer, and Binh T. Pham

Idaho National Laboratory

INL is a U.S. Department of Energy National Laboratory
operated by Battelle Energy Alliance, LLC

INL/RPT-22-66720
Revision 0

Initial Observations from Advanced Gas Reactor (AGR)-5/6/7 Capsule 1

John D. Stempien, Joe J. Palmer, and Binh T. Pham

April 2022

Idaho National Laboratory
Advanced Reactor Technologies
Idaho Falls, Idaho 83415

http://www.art.inl.gov

Prepared for the
U.S. Department of Energy
Office of Nuclear Energy
Under DOE Idaho Operations Office
Contract DE-AC07-05ID14517

Page intentionally left blank

INL ART Program

Initial Observations from Advanced Gas Reactor (AGR)-5/6/7 Capsule 1

INL/RPT-22-66720
Revision 0

April 2022

Approved by:

Paul Demkowicz	4/13/2022
Paul A. Demkowicz ART AGR Program Technical Director	Date
Travis Mitchell	4/13/2022
Travis R. Mitchell ART Program Manager	Date
Michelle Sharp	4/13/2022
Michelle T. Sharp INL Quality Assurance	Date

ACKNOWLEDGEMENTS

A number of people contributed to the current state of knowledge about AGR-5/6/7 Capsule 1, and this report was written while significant work is still in progress toward that end. Grant Hawkes conducted the thermal analyses referred to in this report and helped the authors to understand and interpret these analyses. Philip Winston helped design fixtures for capsule disassembly and sample recovery, and with Cad Christensen, helped direct test train/capsule disassembly. Cassie Anderson-Thueson and Skyler James are hot cell operators who helped with disassembly, inspection, and organization of recovered fuel and samples. Edward Reber conducted gamma spectrometry of the deposits collected from the outside of the Capsule 1 holder. Glen Papaioannou and staff at Neutron Radiography Reactor (NRAD) collected the neutron radiographs of Segment 1 of the AGR-5/6/7 test train that contained Capsules 1 and 2. Katelyn Wheeler and Katie Hawkins collected precision gamma scanner (PGS) spectra from Segment 1 of the irradiation test train, and Ryan Fronk analyzed those spectra.

CONTENTS

FIGURES

TABLES

Page intentionally left blank

ACRONYMS

AGR	Advanced Gas Reactor
ART	Advanced Reactor Technologies
ATR	Advanced Test Reactor at Idaho National Laboratory
cps	counts per second
EDS	energy dispersive X-ray spectroscopy
EOI	end-of-irradiation
FIMA	fissions per initial heavy metal atom
FPMS	fission product monitoring system
GG	gross gamma
HFEF	Hot Fuels Examination Facility
HTIR	high-temperature irradiation resistant
INL	Idaho National Laboratory
NEFT	northeast flux trap
NRAD	Neutron Radiography Reactor
PALM	powered axial locator mechanism
PGS	precision gamma scanner
PIE	post-irradiation examination
R/B	release-to-birth
SCCM	standard cubic centimeters per minute
SEM	scanning electron microscope
TAVA	time-averaged volume-averaged
TC	thermocouple
TRISO	tristructural isotropic
VEM	visual examination machine

Page intentionally left blank

Initial Observations from Advanced Gas Reactor (AGR)-5/6/7 Capsule 1

1. INTRODUCTION

1.1 Background

The fourth and final irradiation experiment in the Advanced Reactor Technologies (ART) Advanced Gas Reactor (AGR) fuel development and qualification program is designated as AGR-5/6/7. Data collected from the fabrication, irradiation, and post-irradiation examination (PIE) of this tristructural isotropic (TRISO) fuel are intended to serve as the primary data set for the qualification of this fuel for use in high-temperature gas-cooled reactors (INL 2021, Collin 2018). However, data collected from the three preceding irradiations (i.e., AGR-1, AGR-2, and AGR-3/4) may also be used to supplement data collected from AGR-5/6/7.

All components of the AGR-5/6/7 fuel (i.e., uranium carbide/oxide kernels, TRISO coatings, and fuel compacts) were produced on an engineering scale at BWXT (Lynchburg, Virginia USA) according to the fuel specification (Marshall 2017). This fuel was irradiated in the northeast flux trap (NEFT) at the Advanced Test Reactor (ATR) at Idaho National Laboratory (INL) from February 16, 2018, to July 22, 2020 (Pham et al. 2021). Measurements in the fission product monitoring system (FPMS) indicated unexpected and significant numbers of failures of TRISO particles in Capsule 1 near the end of the sixth irradiation cycle (ATR Cycle 166A). In the fourth cycle (ATR Cycle 164B) and beyond, the sweep-gas flow became very low (presumably from degradation of the capsule gas outlet line via an unidentified mechanism), and the program deliberately isolated Capsule 1 from gas flow periodically. In later cycles, attempts to reestablish any kind of flow in Capsule 1 were unsuccessful. With little or no flow through Capsule 1, FPMS measurements and enumerations of failed particles in Capsule 1 were difficult or impossible as was the ability to control the helium/neon gas mixture used for temperature control. Gas flows and fission gas activity in the effluent gas from the other AGR-5/6/7 capsules were also impacted by the Capsule 1 gas flow issues and the large increase in fission gas released from Capsule 1.

Following the completion of the irradiation, the experiment test train was transferred from ATR to the Hot Fuel Examination Facility (HFEF) at the Materials and Fuels Complex at INL for non-destructive and destructive PIE. AGR-5/6/7 PIE is in progress, and significant work on fuel and test train components from all capsules, including Capsule 1, will be completed over the next several years. This document serves as a status report on the state of knowledge surrounding Capsule 1 as of April 2022.

1.2 Capsule 1 Description

The AGR-5/6/7 irradiation test train consisted of five independently instrumented and controlled capsules. Multiple different capsule designs were used within the AGR-5/6/7 test train. The discussions in this section will focus on Capsule 1, but some major characteristics of the other capsules will be mentioned for comparative purposes. Figure 1 shows a schematic of an axial cross section of the assembled test train that was loaded into NEFT at ATR, and Figure 2 shows schematic radial cross sections of each of the five different capsules. The capsules were numbered from the bottom (Capsule 1) to the top (Capsule 5) of the test train. The stainless-steel capsule shells acted as the experiment pressure boundary, separating the experiment from the ATR coolant water that flowed around the outside of the test train. The stainless-steel shells for the capsules were welded together one on top of the other. Figure 2 shows that Capsule 1 had 10 stacks of fuel compacts, and Figure 1 shows that each of these 10 stacks had nine fuel compacts. Capsules 2, 4, and 5 each had four stacks of compacts; however, in Capsule 2, each stack had eight compacts (compared to six compacts per stack in Capsules 4 and 5). Capsule 3 had three compact stacks containing eight compacts each.

Each capsule had an independent helium and neon gas supply to control the temperature within the capsule by varying the gas composition and to sweep gaseous fission gases to the FPMS (Pham et al. 2021). A stainless-steel leadout tube held the experiment in position and contained and protected the gas lines and thermocouple (TC) wiring extending from the test train to the reactor penetration. A number of TCs were installed in each capsule for temperature monitoring. Capsule 1 did not have any through-tubes, but Capsules 2 through 5 each had four through-tubes to accommodate gas lines and TC leads from capsules below them in the test train. Capsule 3 had two graphite holders: an inner holder for the fuel compacts and an outer holder. The other capsules each had only a single graphite holder with a hollow center designed to reduce graphite mass and graphite volumetric heating (Collin 2018). All holders were made from IG-430 graphite. Figure 2 shows a series of nubs on the outside of each capsule shell. These nubs helped to center the test train in NEFT. A set of double nubs (shown in Figure 2 at the 7 o'clock position on each shell) points to the southeast direction and can be used to denote the orientation of the capsules when they were in ATR. Each fuel compact stack is numbered according to Figure 2, and noting the positioning of the compact stacks in relation to the nubs can be used to identify each stack number.

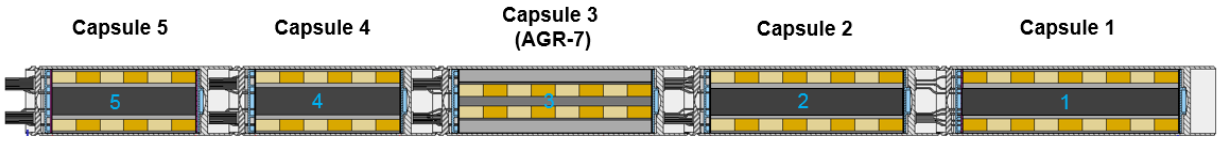

Figure 1. Axial cross-sectional schematic of the AGR-5/6/7 test train.

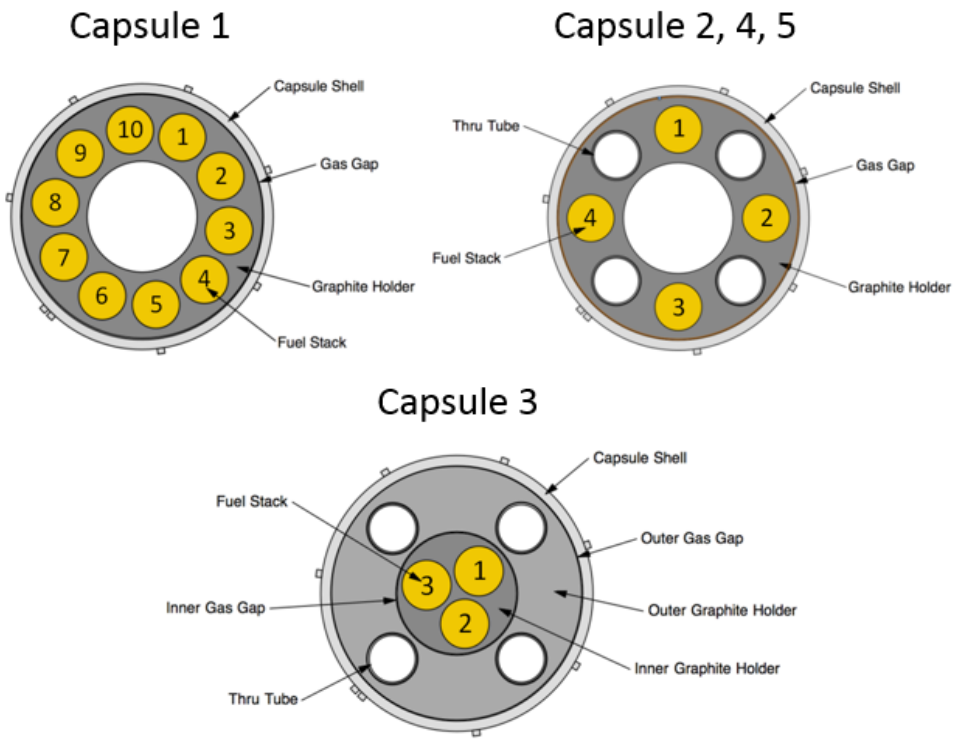

Figure 2. Radial cross sections of the AGR-5/6/7 capsules.

1.2.1 Fuel Compacts

All fuel compacts are approximately 25 mm long and 12.3 mm in diameter. Capsule 1 and Capsule 5 compacts have nominal particle packing fractions of 40%. Capsules 2 through 4 used compacts with 25% particle packing fractions. The particles used in all compacts came from coated particle Lot J52R-16-98005 (Collin 2018).

1.2.2 Thermocouples

A discussion of TC type, selection, and placement is given in the test plan (Collin 2018). The AGR-5/6/7 assembly weldment drawing (DWG 604660) and the drawings for the individual capsules (e.g., DWG 604661 for Capsule 1) provide information on the TCs and their positions within the experiment. TCs penetrated the stainless-steel capsule top heads and extended into small channels in the graphite holders in each capsule. There were four different TC configurations in the AGR-5/6/7 test train as follows:

- Type N (Ni/Cr/Si/Mg wire) with Inconel 600 (Ni/Cr/Fe/Mn alloy) sheath, MgO insulation, and sleeved with Nb (this was the standard baseline TC)
- Type N with Cambridge (Cambridge N) low-drift pure Ni sheath, MgO insulation, and sleeved with Nb in AGR-5/6 capsules and with ZrO_2 in AGR-7 Capsule 3
- Type N with Inconel 600 sheath, Spinel ($MgAl_2O_4$) insulation, and sleeved with Nb
- High-temperature irradiation resistant (Mo/Nb wire) with Nb sheath, Al_2O_3 insulation, and sleeved with Mo (High Temperature Irradiation Resistant [HTIR]).

Capsule 1 utilized one Spinel Type N, seven Cambridge Type N, and nine HTIR Type N TCs. Capsule 1 did not use any of the standard baseline Type N TCs. Capsules 2, 4, and 5 all used the standard TCs exclusively. Capsule 3 used the same types of TCs as Capsule 1 with one difference in the Cambridge Type N TC assemblies: in Capsule 1, the Cambridge Type N TCs utilized a Nb sleeve outside of the Ni sheath, but in Capsule 3, the Cambridge Type N TCs used a ZrO_2 sleeve instead of Nb because of the higher expected temperatures in Capsule 3.

Figure 3 shows a top-down drawing of the Capsule 1 graphite holder along with the locations of the TC penetrations machined into the graphite holder, the 10 fuel stacks, and a table of the Capsule 1 TC IDs, types, and depth of TC junction penetration into the holder, measured from the top.

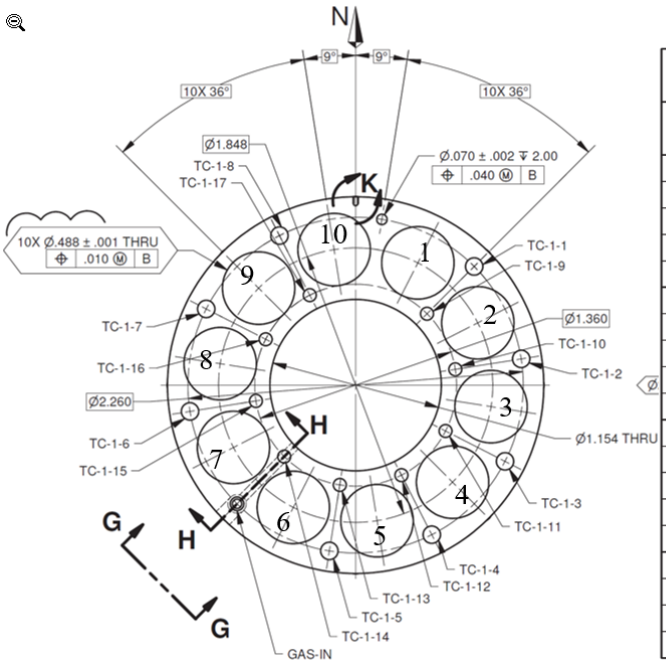

TC/GAS LINE PENETRATION

TC OR GAS LINE #	DIM "A" (PENETRATION LENGTH)	ITEM #	TYPE OR MATERIAL
TC-1-1	2.4	22	CAMB-N
TC-1-2	2.4	24	SPINEL-N
TC-1-3	2.4	22	CAMB-N
TC-1-4	2.4	22	CAMB-N
TC-1-5	4.4	22	CAMB-N
TC-1-6	6.4	22	CAMB-N
TC-1-7	8.4	22	CAMB-N
TC-1-8	8.4	22	CAMB-N
TC-1-9	6.4	23	HTIR-TC
TC-1-10	2.4	23	HTIR-TC
TC-1-11	2.4	23	HTIR-TC
TC-1-12	4.4	23	HTIR-TC
TC-1-13	4.4	23	HTIR-TC
TC-1-14	2.4	23	HTIR-TC
TC-1-15	6.4	23	HTIR-TC
TC-1-16	2.4	23	HTIR-TC
TC-1-17	8.4	23	HTIR-TC
GAS-IN	4.0	31	304 SST
GAS-OUT	(.185)	31	304 SST

Figure 3. Excerpts from the Capsule 1 drawing package (DWG 604661) showing some features of the graphite holder and the TCs inserted into the graphite holder. Annotations for the fuel stack numbers were added.

1.2.3 Miscellaneous Capsule Components

During assembly of the test train prior to irradiation, the insides of the stainless-steel shells were coated in a thin film of Neolube No. 1 to increase the emissivity of the stainless-steel. It was estimated the thickness of this film was 0.0015 to 0.0018 in. (Hawkes 2022). Neolube is a dilute colloidal suspension of graphite particles and a thermoplastic resin in isopropanol. After the initial application of Neolube, the instructions call for it to be allowed to air-dry, resulting in a film that can function as a dry lubricant and an anti-seize compound. According to the manufacturer, Neolube No. 1 has seen extensive use in nuclear applications with a service temperature of about 200°C and an allowable intermittent temperature of about 450°C. Recent tests conducted by the AGR program at INL involved heating Neolube No. 1 in helium to 1000°C using a thermogravimetric analyzer. The weight loss was about 2% in heating from room temperature to 280°C. From 280–350°C, weight loss was an additional 20%. By 1000°C, the Neolube sample had lost about 30% of its original mass.

Each capsule had a gas inlet and outlet, as well as bulkheads at the top and bottom, referred to in this report as the “top head” and “bottom head”. The gas inlet line penetrated the capsule top head and ran in a small channel in the graphite holder to the bottom of the specific capsule to which it was supplying gas. In each capsule, the gas outlet line barely penetrated the capsule top head to access the plenum at the top of the capsule.

Each capsule also had an assortment of smaller items used to support and position the compacts and graphite compact holders. This included spacers, disks, insulators, gamma “heaters,” and the Capsule 1 Inconel “wave spring”. The spacers are made of zirconia or graphite. The disks are made of Grafoil. The insulators are made of zirconia. Capsule 3 heaters are made of tungsten. The self-powered neutron detectors in Capsules 4 and 5 were inside titanium tubes, which were inside the through-tubes.

2. OBSERVATIONS FROM IRRADIATION IN ATR

The AGR-5/6/7 experiment was irradiated in the NEFT of ATR, which significantly enhanced test capabilities for the combined irradiation campaigns. The irradiation spanned nine ATR cycles (162B–168A) over two and a half years and a total of approximately 360.9 effective full-power days. Fuel compacts in Capsule 1 reached burnup values ranging from 5.66 to 15.26% fissions per initial heavy metal atom (FIMA) and fast neutron fluences ranging from 1.62 to 4.40 × 10^{25} n/m^2 (E >0.18 MeV). The time-averaged volume-averaged (TAVA) fuel temperature averaged over all compacts in Capsule 1 was 1001°C excluding days with significantly lower temperature during the two short powered axial locator mechanism (PALM) cycles (163A and 167A) and assuming zero neon fraction in Capsule 1 during the last cycle, 168A.[a]

Gas line problems in Capsule 1 started from the fourth cycle (164B), and all 17 TCs had failed before the end of the sixth cycle (166A), complicating fuel temperature control and fission gas measurements for Capsule 1 during the second half of irradiation. In addition, a few hundred in-pile particle failures were estimated for Capsule 1 by the end of Cycle 166A based on available fission gas release-to-birth (R/B) data, but the total number of failures is unknown because the Capsule 1 gamma detectors became saturated before the end of Cycle 166A (making further measurement impossible) and because of the lack of fission gas-release data in the later cycles (a result of terminating gas flow for this capsule during reactor operation for the remainder of the experiment). The true number of TRISO particle failures in Capsules 1 has been estimated to be on the order of thousands (Scates 2021).

2.1 Temperatures

The Abaqus finite-element stress and heat transfer code was used to perform the daily as-run thermal analysis for the AGR-5/6/7 capsules (Hawkes 2022). The AGR-5/6/7 thermal model provides detailed temperatures calculated for each finite-element volume of the entire test train. These are used to calculate Capsule 1 daily instantaneous (Figure 4) and time-averaged (Figure 5) values for minimum, volume-averaged, and maximum (or peak) fuel temperatures for each time step (or each day). The fractions of fuel in each capsule with calculated irradiation temperatures within different temperature ranges are shown in Figure 6. By design, most of the AGR-5/6/7 fuel with irradiation temperatures between 900 and 1250°C was in Capsule 1. Some fuel with irradiation temperatures between 900 and 1050°C was also in Capsule 2 and 4.

During the last ATR cycle (Cycle 168A), the gas flow for Capsule 1 was isolated after purging the capsule with pure neon flow before powering up for this cycle. However, some of the gas from the leadout entered Capsule 1 through a break in the capsule gas line, which could increase the Capsule 1 neon fraction from zero to the leadout neon fraction. This leak rate is unknown, and therefore the Capsule 1 neon fraction was not known with certainty during Cycle 168A, which led to a high uncertainty in Capsule 1 calculated temperatures. Therefore, Capsule 1 temperatures can only be bounded from the minimum value at zero neon fraction (darker colors in Figure 4 and Figure 5) and the maximum value at the lead-out neon fraction (lighter colors in Figure 4 and Figure 5). The instantaneous temperature differences between these two cases during Cycle 168A are more than 200°C.

[a] The temperatures discussed in this section are those calculated in the as-run thermal analysis (Hawkes 2022), and do not take into consideration potential displacement of capsule components from their intended positions as discussed in subsequent sections. Additional thermal analyses may be required to determine the impact of these changes to fuel temperature.

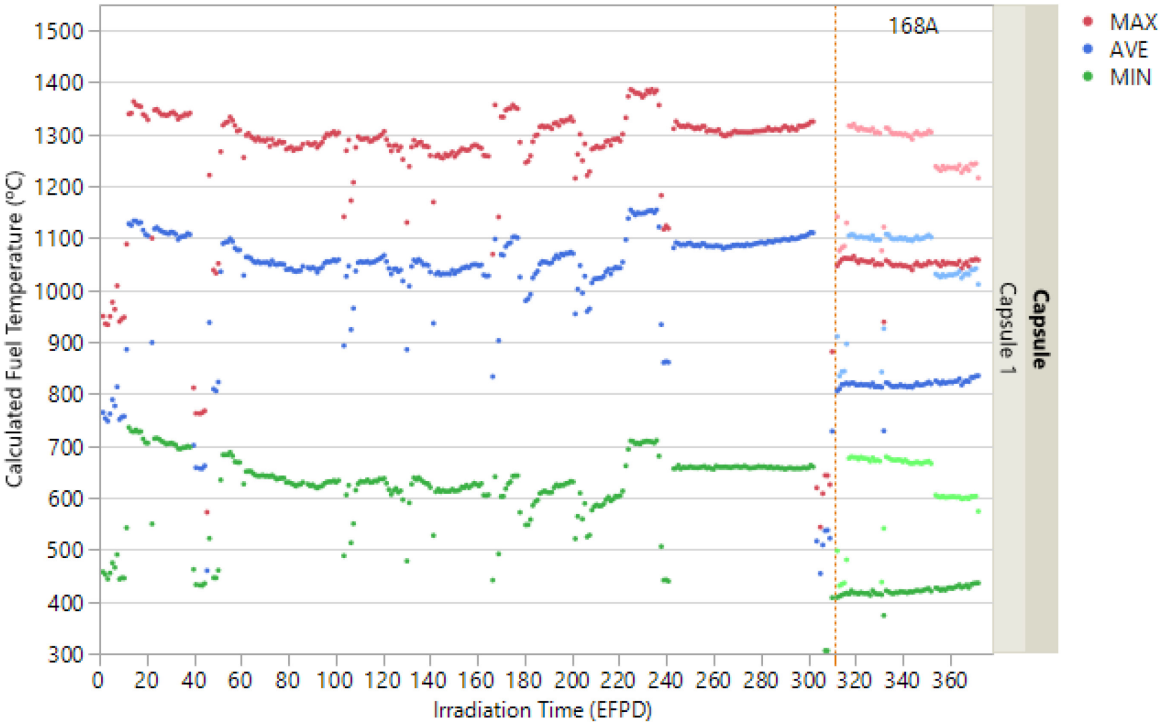

Figure 4. Calculated daily instantaneous minimum, maximum, and volume-averaged fuel temperatures (light color dots are for the assumed lead-out neon fraction instead of zero for Cycle 168A).

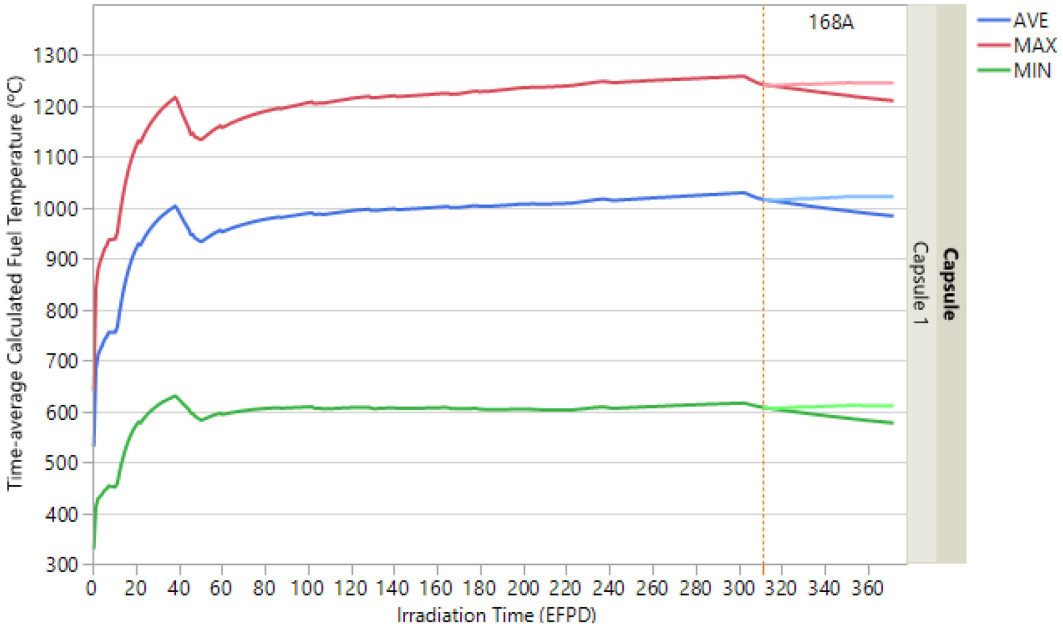

Figure 5. Calculated time-averaged minimum, maximum, and volume-averaged fuel temperatures (light color lines are for the assumed lead-out neon fraction instead of zero for Cycle 168A).

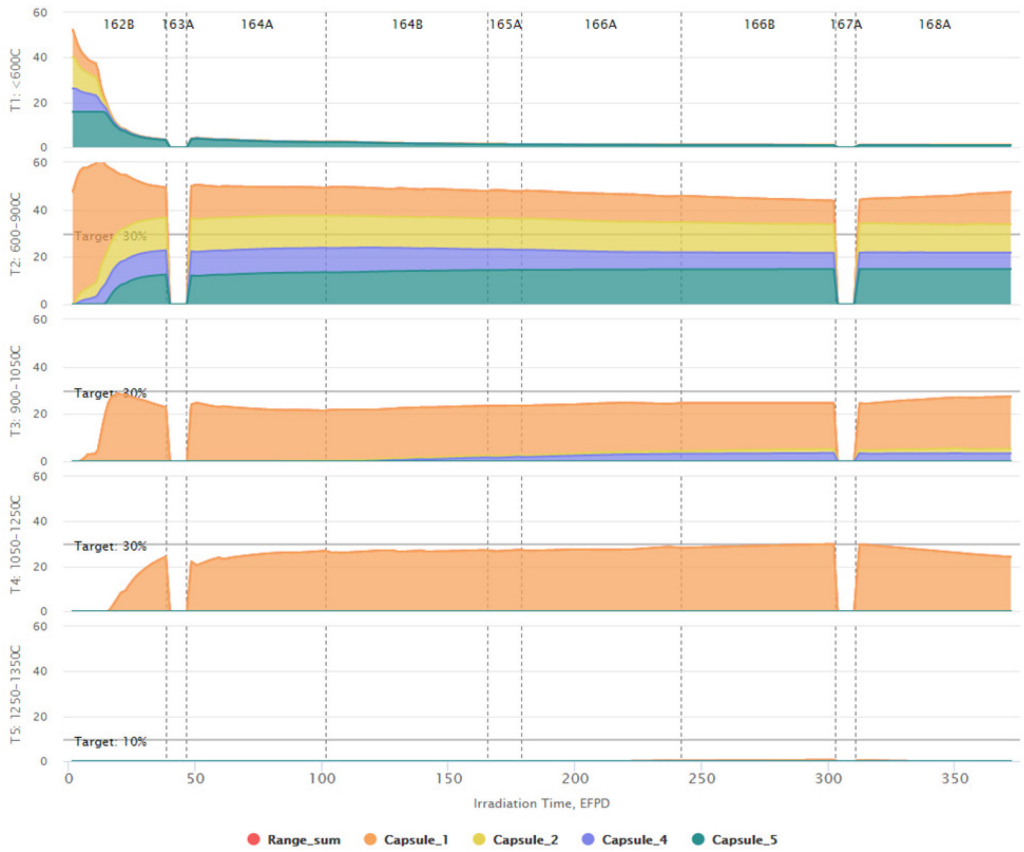

Figure 6. Fractions of fuel in various TAVA temperature ranges for fuel in each capsule excluding the high-temperature Capsule 3 and excluding the low-power PALM cycles 163A and 167A.

The time-average temperature calculations were performed for two scenarios: (1) including all nine cycles, and (2) excluding the two low-power PALM cycles (Cycles 163A and 167A) (Pham et al. 2021). Given how short the two low-power PALM cycles were, the time-average values of the volume-average and peak compact temperatures at the end of irradiation (EOI) are summarized in Table 1 by excluding these two PALM cycles. The instantaneous peak temperature from all volumes and all timesteps for each capsule and experiment are also included in Table 1. The burnup, fluence, minimum temperature, volume-averaged temperature, and peak time-averaged temperatures at the EOI are presented in Appendix A for all 90 compacts in Capsule 1.

Table 1. Capsule 1 peak and time-average temperature (°C). The two time-average values correspond to values without the inclusion of data from low-power PALM Cycles 163A and 167A.

Capsule and Experiment	Instantaneous Peak Temperature	Time-average Minimum Temperature	Time-average Average Temperature	Time-average Peak Temperature
All Capsule 1 compacts (zero Ne)	1386	588	1001	1231
All Capsule 1 compacts (lead-out Ne)	1386	624	1041	1267

2.2 Gas Flows

Sweep-gas parameters are mass-flow rates for each constituent gas and moisture content. The mass-flow rates for each constituent gas, measured at the inlet line for each capsule and the lead out, are referred to as inlet flow rates; the total mass-flow rates, measured at each capsule outlet line, are referred to as outlet flow rates. An additional mass-flow rate is measured at the FPMS. By design, a nominal helium/neon mixture flow at a higher pressure than the capsule pressure was provided via a mass-flow controller into the lead-out cavity, which then flowed into the common plenums between capsules. The intent of this design was to prevent capsule-to-capsule cross gas leakage ensuring fission-gas signatures remain separated by capsule.

However, Capsule 1 gas line problems started from Cycle 164B and had a significant impact on the interpretation of the fission gas release data. A clog and then a crack formed in the Capsule 1 outlet line that prevented its fission gases from sweeping out to the detector as intended. Thus, some of the Capsule 1 fission gas diffused out, contaminated gas in the lead out, and then entered other capsules. To mitigate this issue, the lead-out pressure was reduced to below the capsule pressures and the lead-out outlet isolation valve was opened, allowing the lead-out contaminated gas to flow to spare Detector 6. This arrangement allowed some gas flow from Capsules 2–5 to the lead out, limiting fission gas leakage into Capsules 2–5 from the lead out. Details of the Capsule 1 gas line problem were documented in Engineering Calculations and Analysis Report (ECAR)-5114 (Nelson, 2020).

Capsule 1 gas flow rates from Cycle 164B were significantly lower and were largely at zero during two cycles, Cycles166B and 168A due to gas line isolation (Figure 7). In addition, the outlet and FPMS flow rates for the lead out were zero for the first six cycles 162B–166A when its outlet isolation valve was closed as intended. However, they became high-flow rates during the last three cycles 166B–168A when the lead-out outlet isolation valve was opened to prevent gas leakage to Capsules 2–5 (Figure 8).

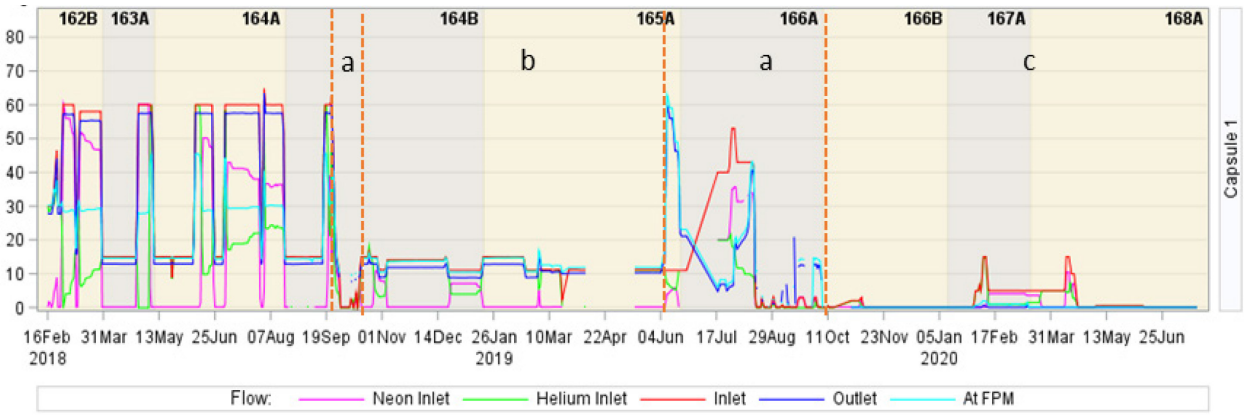

Figure 7. Capsule sweep-gas flow rates (in standard cubic centimeters per minute [SCCM]) with Capsule 1 flow history: (a) intermittent flow, (b) stabilized low flow rate, and (c) mostly isolated gas line with an unsuccessful attempt to reestablish flow during Cycles 167A and 168A.

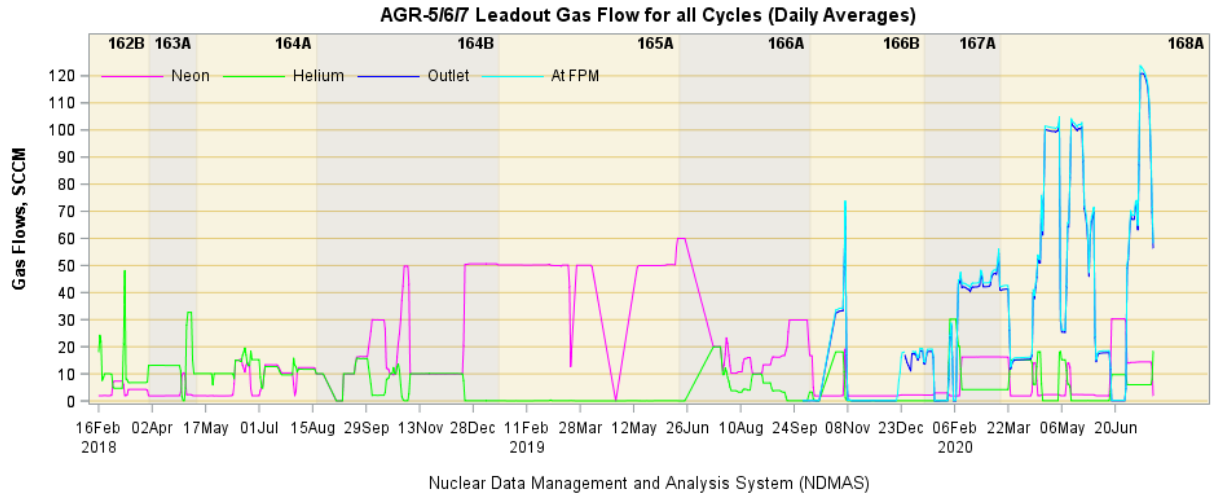

Figure 8. Lead-out sweep-gas flow rates: outlet isolation valve was opened from Cycle 166B.

2.3 Fission Gas Releases

The irradiation performance of a nuclear fuel test is typically evaluated using the R/B ratio, which is the ratio of the released activity of an isotope from the fuel to the predicted creation rate of the isotope during irradiation (or birthrate). The as-run fission gas release analysis results for AGR-5/6/7 experiment are documented in ECAR-5352 (Scates, 2021), which includes R/B data for the 12 isotopes, Kr-85m, Kr-87, Kr-88, Kr-89, Kr-90, Xe-131m, Xe-133, Xe-135, Xe-135m, Xe-137, Xe-138, and Xe-139.

During the first five cycles (162B – 165A), the fission-gas isotope R/B ratios were stable in the 10^{-8}–10^{-6} range for most isotopes (Figure 9 and Figure 10), except R/Bs for the longest isotope Xe-131m. High exposed kernel fraction and high fuel particle temperatures in Capsule 1 led to a maximum R/B value of around 2×10^{-6} for Kr-85m. Also, no in-pile particle failures were observed before Cycle 166A based on the gross gamma (GG) counts (Figure 11).

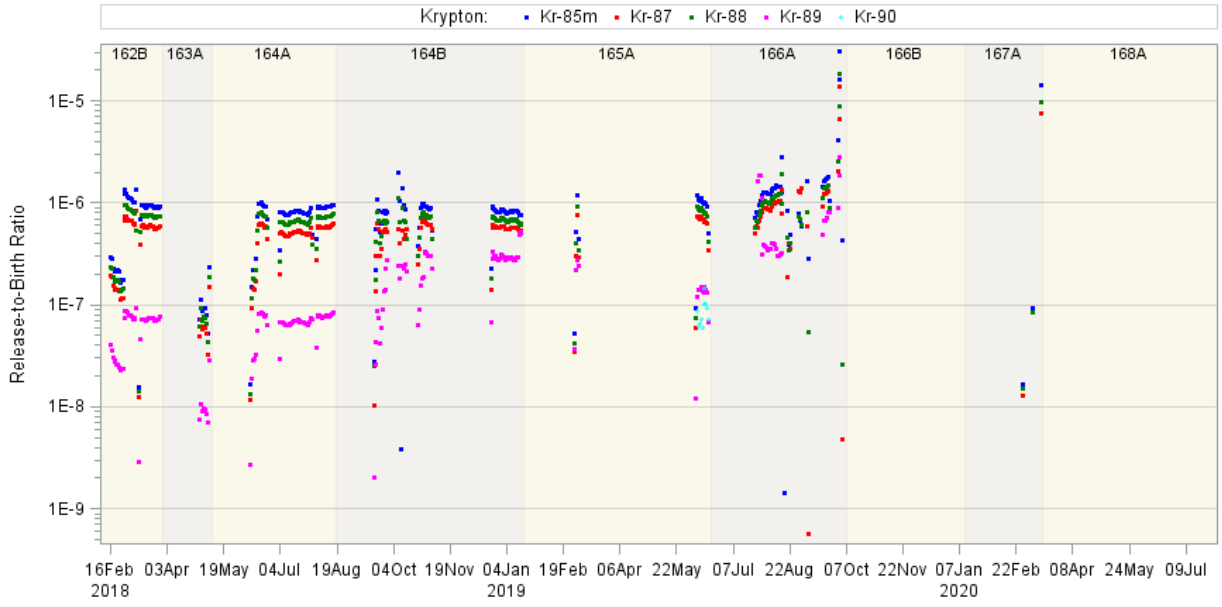

Figure 9. Capsule 1 measured R/B for krypton isotopes.

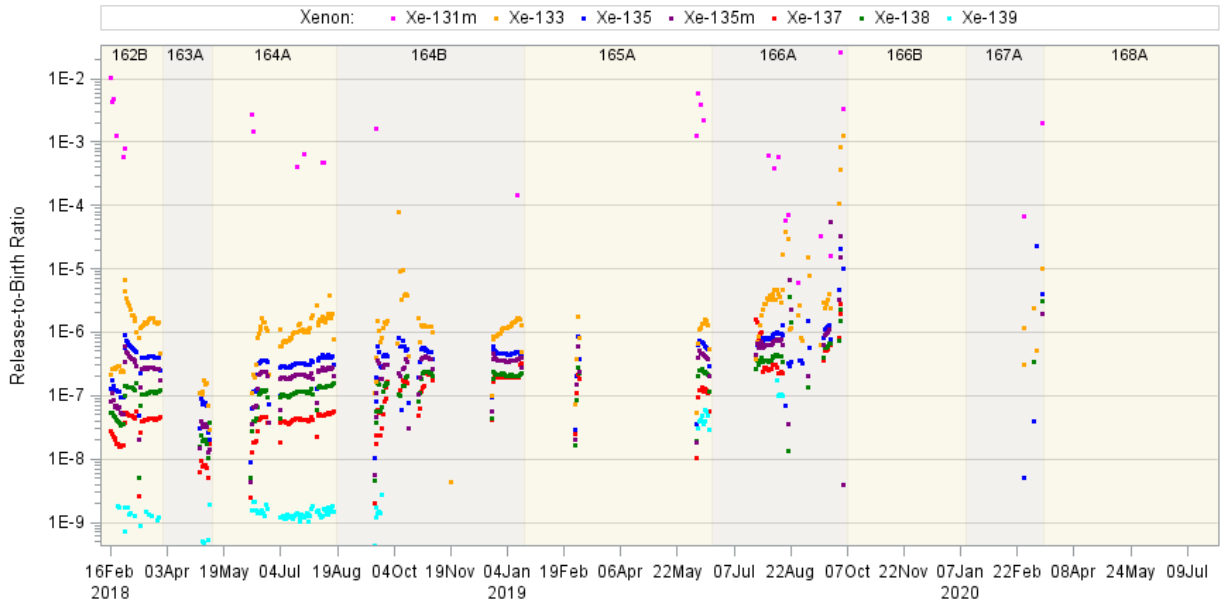

Figure 10. Capsule 1 measured R/B for xenon isotopes.

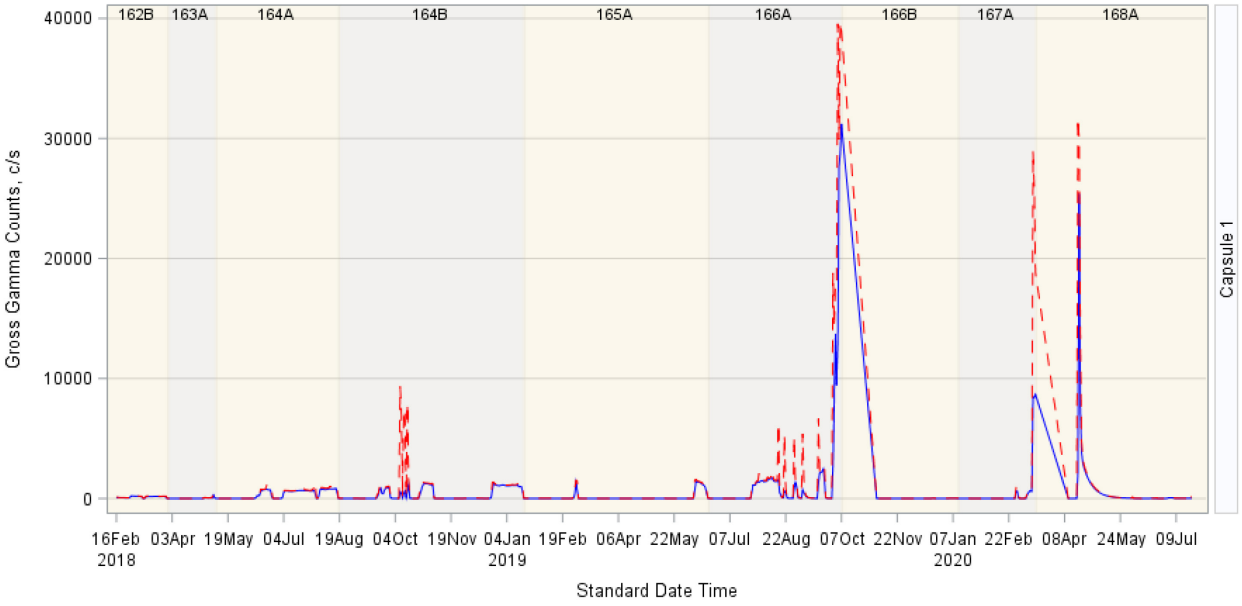

Figure 11. Capsule 1 daily average (blue line) and maximum (red line) GG counts.

The fission gas release in Capsule 1 started to increase for all isotopes during Cycle 166A when a large number of in-pile particle failures occurred by the end of this cycle (Figure 9 and Figure 10). In addition, the worsening of the gas line problem led to total isolation of the gas flow to Capsule 1 and prevented fission gas release measurements during the last three cycles. A large number of spikes in the GG count data is evident for Capsule 1 during the last week of Cycle 166A when Capsule 1 outlet flow resumed as shown in plots of 5-minute average and peak GG counts in Figure 12. These spikes and subsequent increase in averages indicate that multiple particle failures had occurred in Capsule 1. From August 4 to October 3, 2019, Xe-133 activity data indicate that more than 1,000 particle failures may have occurred (Scates 2021). Data from the germanium detectors became unreliable after October 3 because of the increased detector deadtime which led to complete saturation. Thus, the final number of in-pile particle failures in Capsule 1 by the EOI is unknown due to absence of the fission product release data.

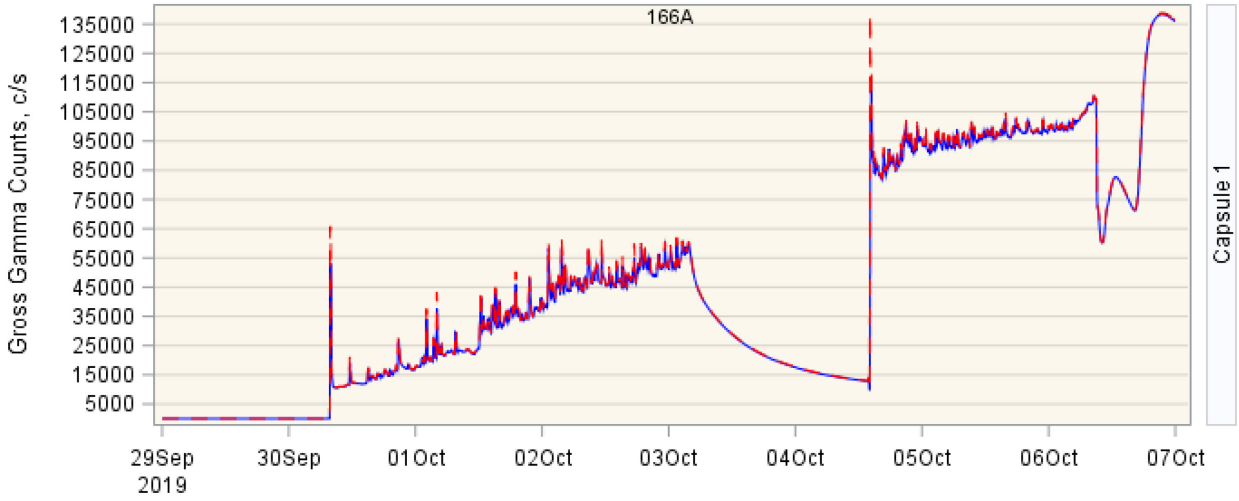

Figure 12. 5-minute average (blue line) and peak (red line) GG counts during the last week of ATR Cycle 168A.

3. OBSERVATIONS FROM PIE

A host of normal PIE processes are planned for AGR-5/6/7, and Figure 13 shows a flowchart of some of these major activities (Stempien 2020). Items that have been completed and are currently in progress for Capsule 1 have been circled. A couple additional activities such as elemental analysis of deposits found on the outside of the Capsule 1 graphite holder are in progress. Items such as compact deconsolidations, post-irradiation heating tests, cross sectioning, ceramography, and x-ray computed tomography of particles and compacts are also planned and are included under the title “Destructive exams and heating tests” in Figure 13.

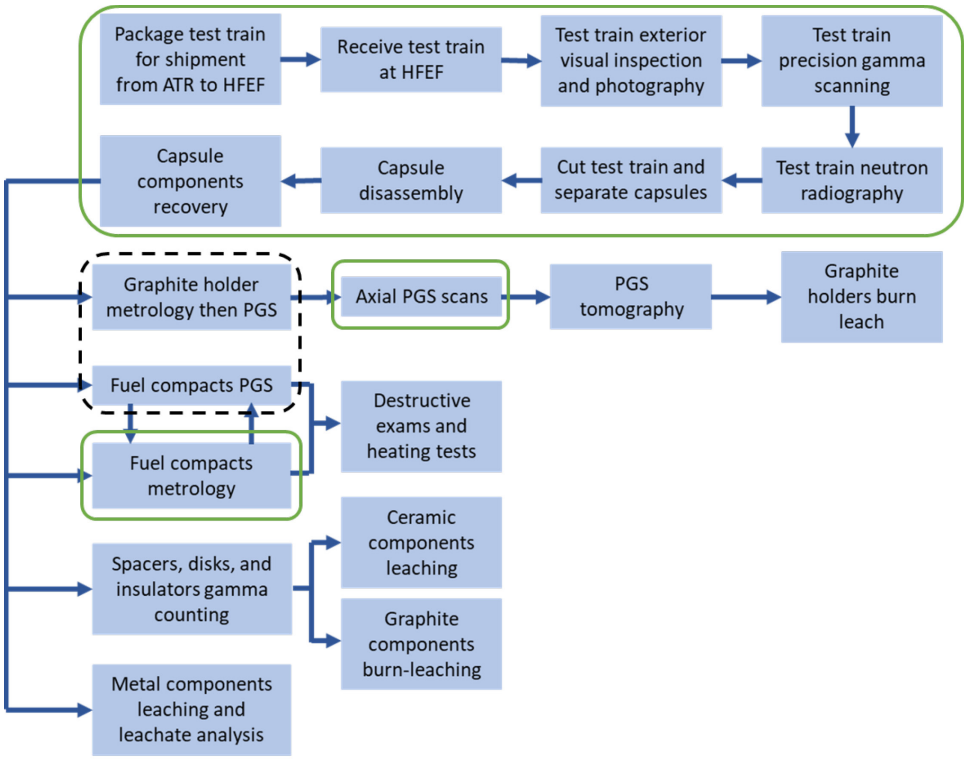

Figure 13. Flow chart showing basic PIE processes. Items circled in a solid green line have been completed for Capsule 1. Items circled in a black dashed line are still in progress for Capsule 1.

3.1 Non-destructive Examinations of the Intact Capsule 1

3.1.1 External Visual

After irradiation at ATR, the AGR-5/6/7 test train was cut into two segments. Segment 1 contained Capsules 1 and 2 and what the drawings refer to as the "bottom hemisphere." Segment 2 contained Capsules 3 through 5. Segment 1 was transferred from ATR to the main hot cell at HFEF where it was photographed and examined. Figure 14 shows a montage of six photos taken along the length of Segment 1 in the vicinity of Capsule 1. The outside of the stainless-steel shell has a series of standoffs referred to as nubs. The double nubs, which faced the camera for the montage shown in Figure 14, were oriented in the southwest direction when the experiment was in NEFT. Three more sets of photos were taken after rotating the test train in three 90-degree increments. In all exams the test train stainless-steel pressure boundary was intact and no abnormal coloring or evidence of test train degradation was noted. Some small scratches and light abrasions commensurate with remote manipulations of the test train in nuclear facilities were observed on the outside of the test train. All welds appeared intact and in good condition. The weld between the bottom of Capsule 1 and the top of the bottom hemisphere was ground flush with the stainless-steel shell when the test train was fabricated and it could not be visually distinguished from the shell material.

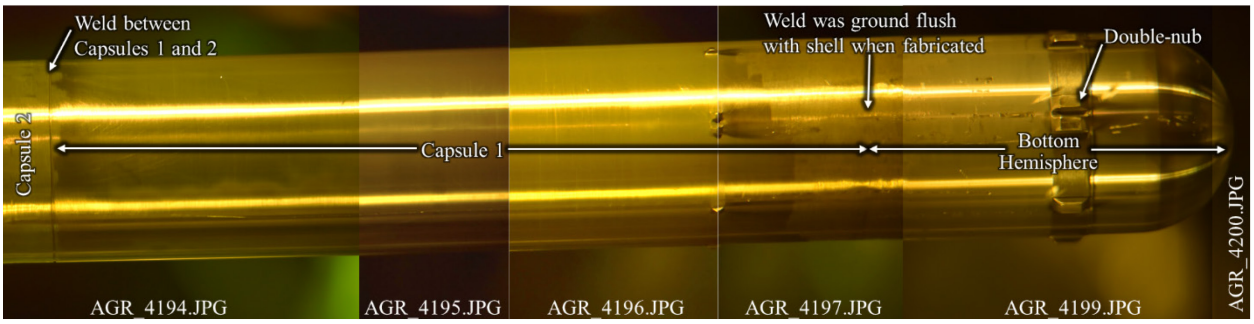

Figure 14. Montage of six photos of Segment 1 of the AGR-5/6/7 test train taken through the hot cell window. Abrupt color changes from left to right are artifacts from combining multiple photos taken at different locations with nonuniform lighting along the test train.

3.1.2 Neutron Radiography

Segment 1 of the test train was moved to the lower level of HFEF for examinations by neutron radiography at the Neutron Radiography (NRAD) reactor. The test train was suspended in front of a neutron beam line, and indium and dysprosium films behind the test train registered transmitted epithermal and thermal neutrons, respectively. Figure 15 shows thermal and epithermal neutron radiographs of AGR-5/6/7 Capsule 1 taken at two orientations 90° apart. Figure 16 shows a montage of thermal neutron radiographs adjusted for brightness and contrast to make the nine levels of compacts more easily visible. The radiographs in Figure 17 show the very top of Capsule 1 along with the gas lines that extend out of the top of Capsule 1 and into the Capsule 2 through-tubes. The fuel compacts are relatively low-density and do not appreciably attenuate the NRAD neutrons; thus, there is not much contrast or detail available from this analysis. Nevertheless, there were no signs of fuel degradation, and aside from the apparent crack in the bottom ZrO_2 spacer, there were no signs of test train degradation.

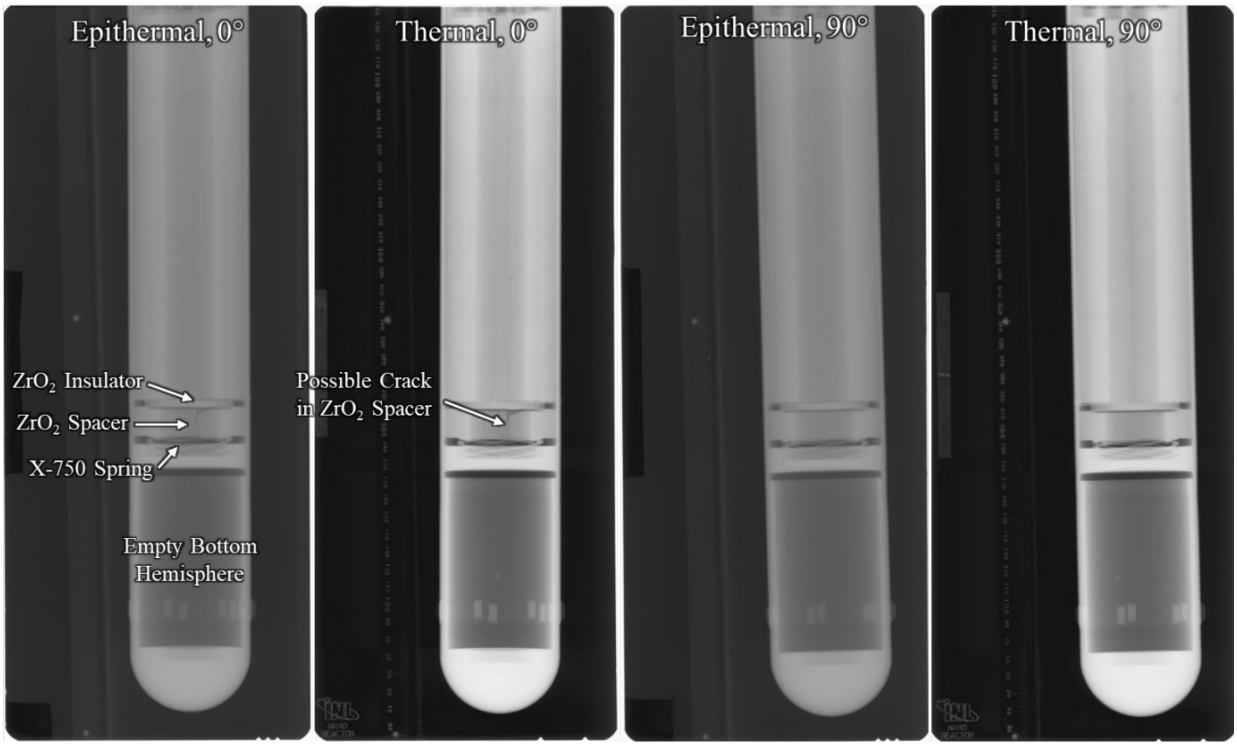

Figure 15. Thermal and epithermal neutron radiographs of AGR-5/6/7 Capsule 1 taken at two orientations 90° apart.

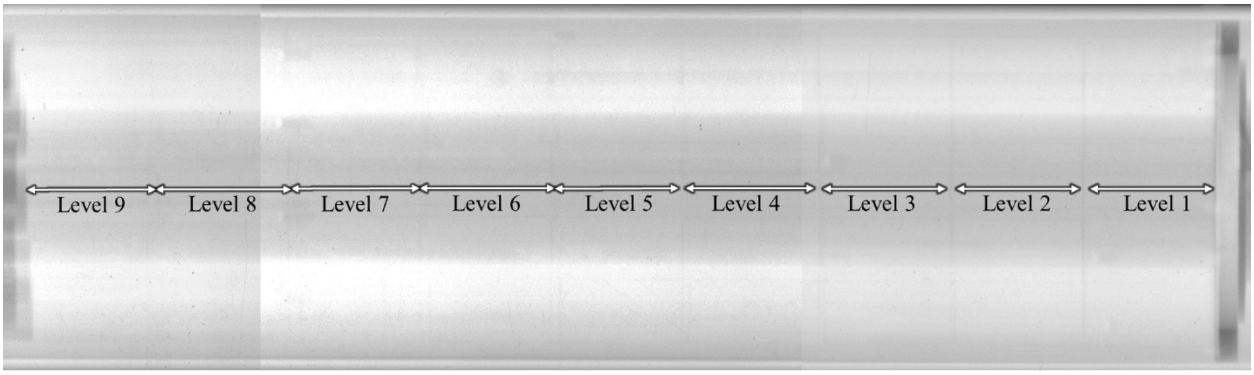

Figure 16. Montage of cropped thermal neutron radiographs adjusted for brightness and contrast to better show the individual levels of compacts in Capsule 1.

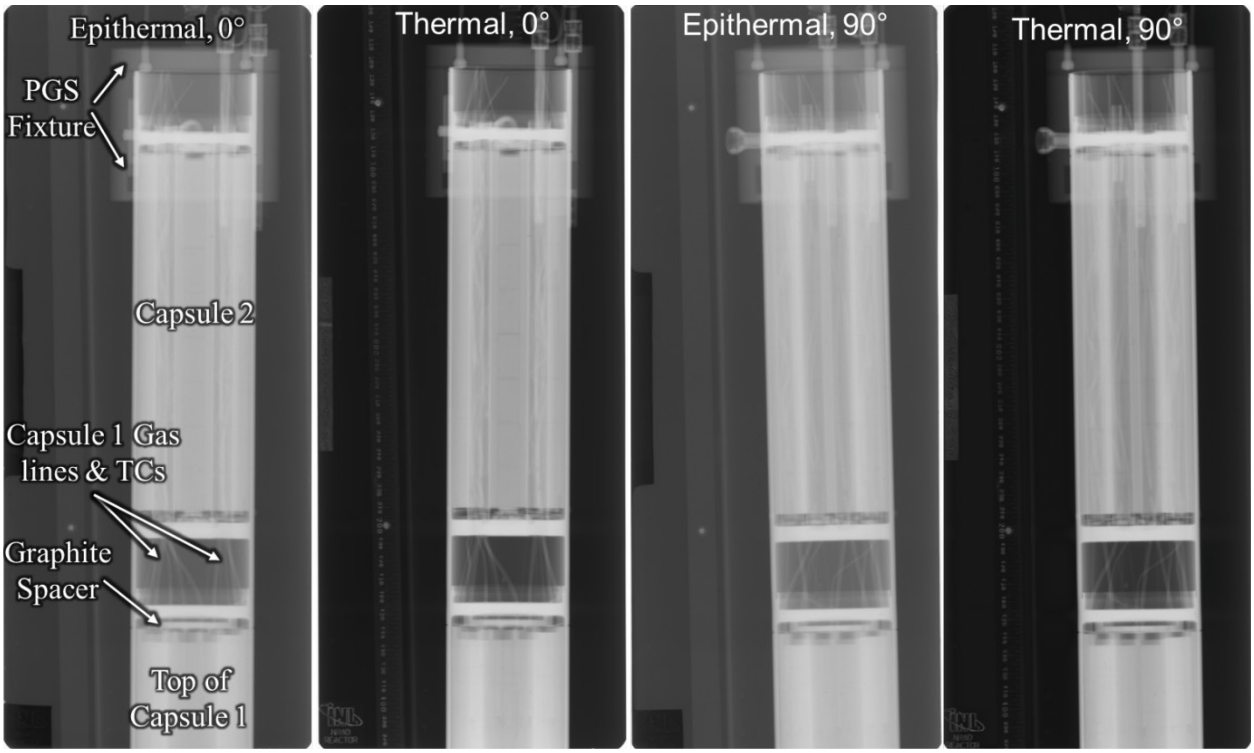

Figure 17. Neutron radiographs showing the top of Capsule 1 and the gas lines and TCs that extend out the top of Capsule 1 and into the Capsule 2 through-tubes.

3.1.3 Gamma Spectroscopy

After radiography, Segment 1 of the test train was moved to the precision gamma scanner (PGS) at the HFEF main cell. The PGS gamma detector system consists of a digital multichannel analyzer and a high-purity germanium detector that is surrounded by a Compton suppression detector. The collimator is approximately 2.13 m long with an aperture that has a fixed width of 2.22 cm and a variable height of 0.254 to 0.00254 cm. Segment 1 was suspended in front of the collimator and moved vertically in a plane parallel to the face of the collimator. Two top-to-bottom scans of this segment of the test train were made, one on the left side and one on the right side.

Figure 18 shows the total gamma count rate (in units of counts per second) from along the right side of the test train. The left-side scan was virtually identical. Areas with high gamma count rates indicate the presence of substantial Co-60 from neutron activation of the stainless-steel test train capsule heads at the top and bottom of each capsule. Within Capsule 1, the total gamma count rate drops from top to bottom due to lower burnup in the fuel and less activation of the stainless steel in accordance with the neutron flux shape in ATR. AGR-5/6/7 compacts were stacked on top of each other, and each capsule contained multiple stacks of compacts. In Capsule 1, for example, there were ten stacks of nine compacts. Small, regularly-spaced dips in the gamma count rate indicate where two compacts are in contact. There are no indications that fuel or interior components of the capsules relocated during irradiation or handling and transportation of the test train.

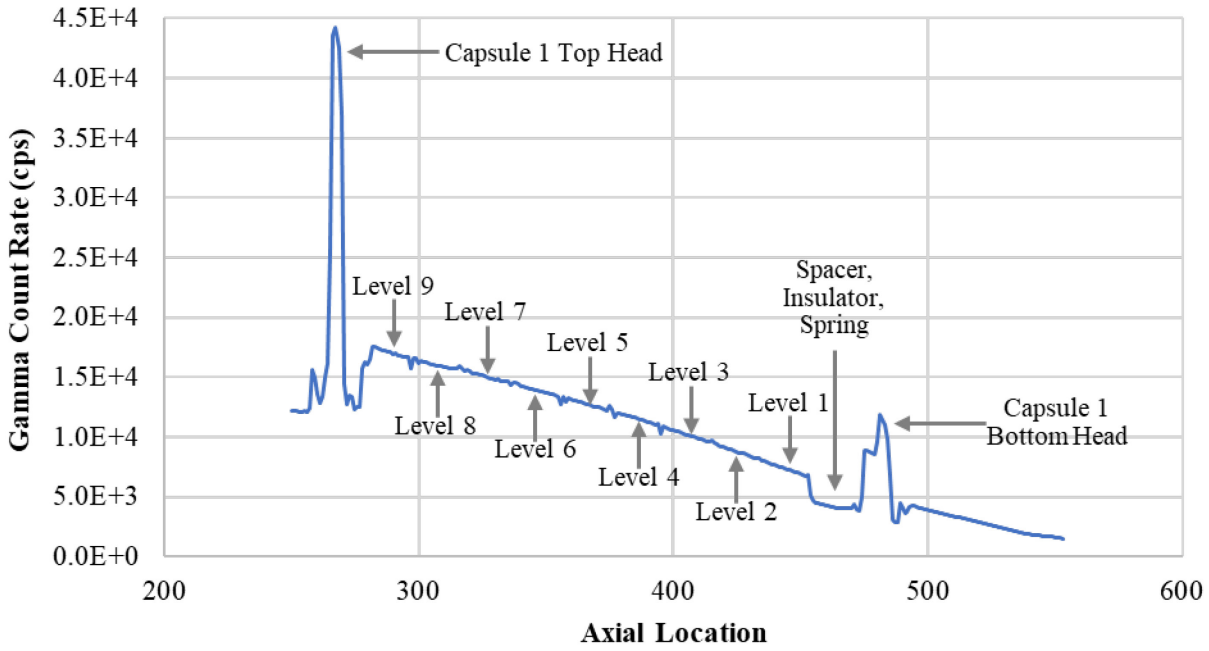

Figure 18. Total gamma count rate in units of counts per second (cps) detected via PGS along the length of the intact Capsule 1. Major identifiable features are annotated.

3.2 Capsule Disassembly

Segment 1 of the test train, composed of Capsules 1 and 2, was clamped into the disassembly table, and a pneumatic pipe cutter was employed to cut the stainless-steel shell in the area between the top of Capsule 1 and the bottom of Capsule 2. After this cut had been made, Capsule 2 could be pulled away from Capsule 1, exposing the TCs and gas lines that exited the top of the Capsule 1 top head. Figure 19 shows a photo of the initial separation of Capsules 1 and 2. Figure 20 shows the removal of the top head from Capsule 1. The top spacer, two Grafoil discs, and TCs were visible at this stage.

Next, cuts were made to remove the bottom head. Figure 21 shows the removal of the bottom head along with views of the interior of the bottom head and the wave spring. The interiors of both the top head (not shown) and the bottom head (shown in Figure 21) appear to have a dark substance with interspersed light-colored spots. It is not clear what this substance is; however, it was not unusual to observe dark substances adhered to the capsule shells and heads in prior AGR irradiations (Demkowicz et al. 2011; Ploger et al. 2015; Stempien et al. 2016).

After removing the bottom head, the bottom spacer could not be removed, and this prevented pushout of the graphite holder. A second cut, in between the bottom of the graphite holder and the top of the bottom spacer, was made to enable removal of the spacer. Burrs left from cutting the capsule shell prevented pushout of the graphite holder; thus, the holder was temporarily left in place so that the compacts could be pushed out. Extra deburring steps using modified tools were required before the graphite holder could be pushed out of the Capsule 1 shell.

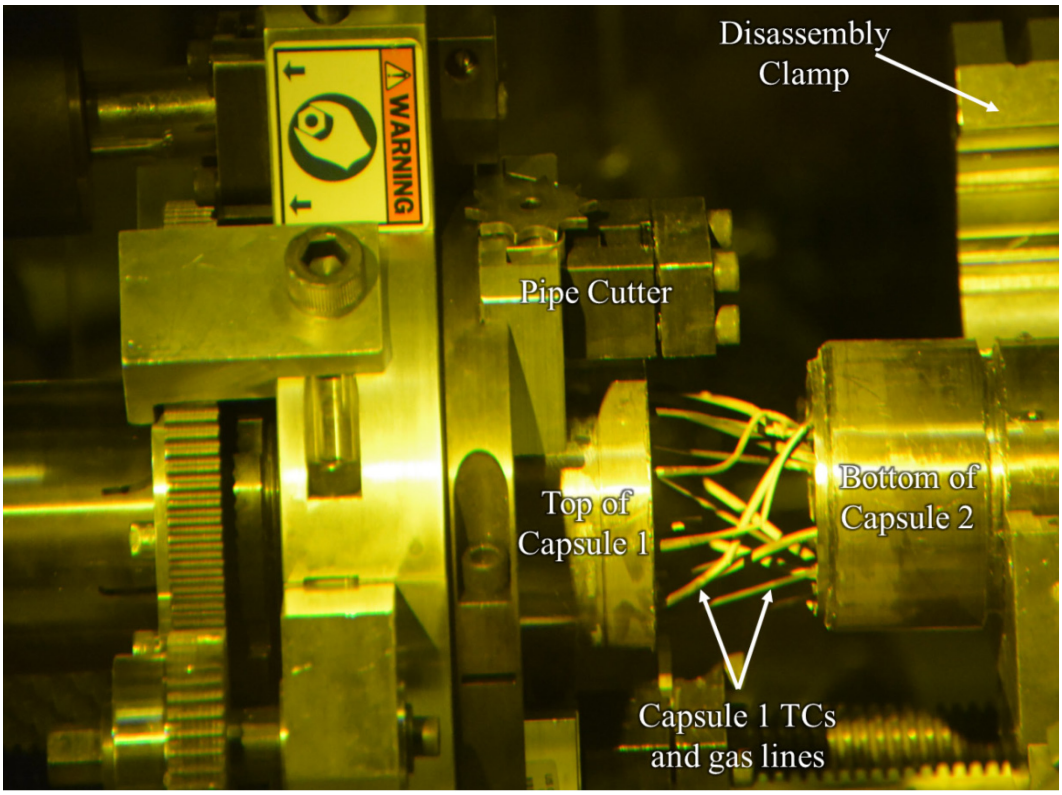

Figure 19. Separation of Capsules 1 and 2. Photo taken through the hot cell window at HFEF.

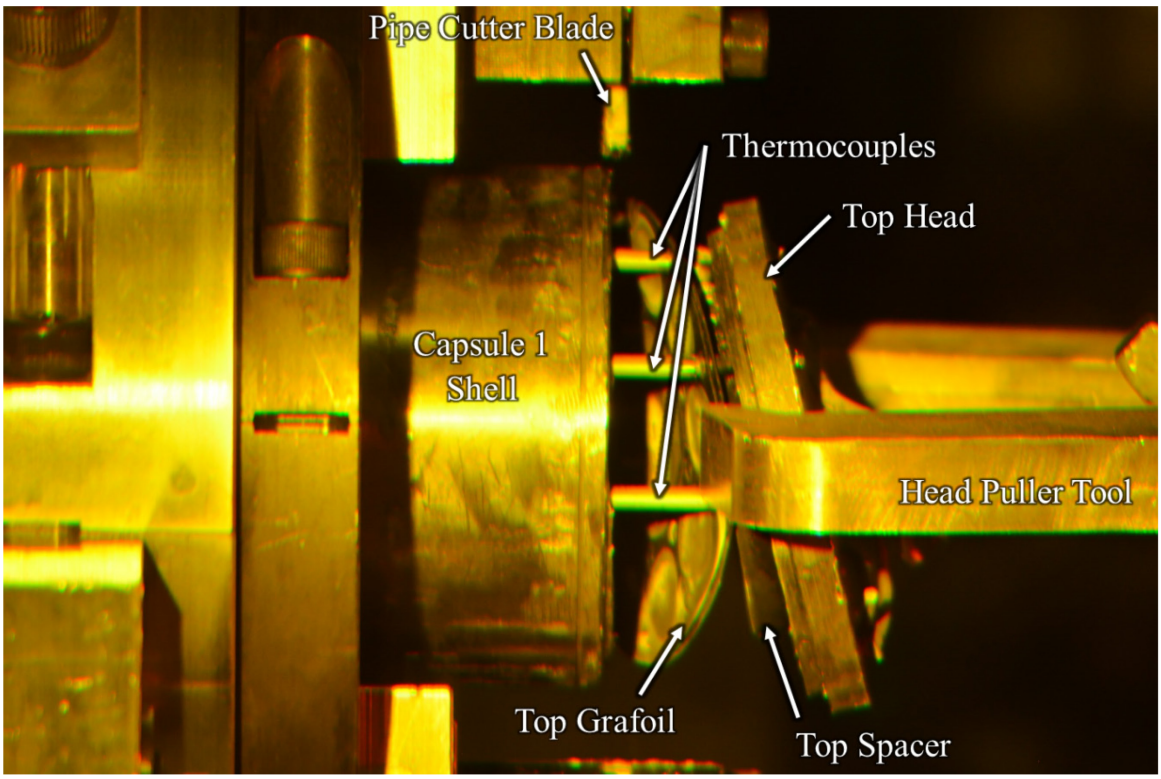

Figure 20. Removal of the Capsule 1 top head. Photo taken through the hot cell window at HFEF.

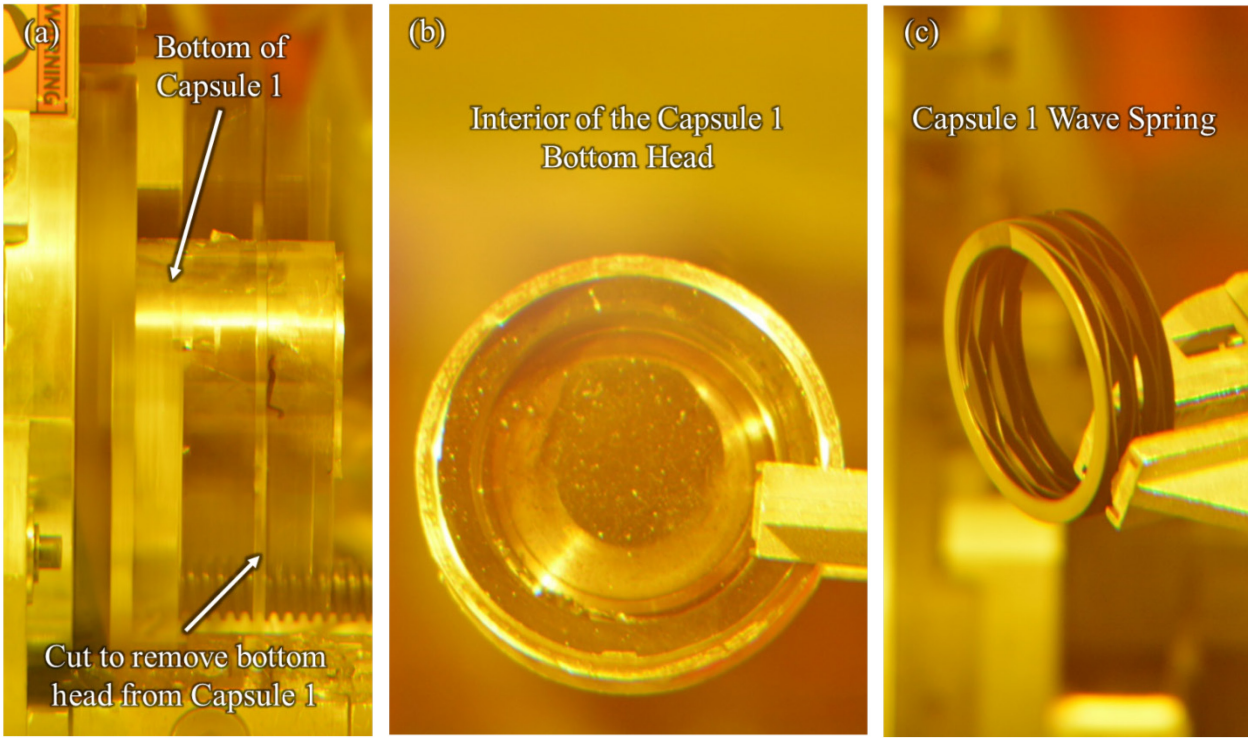

Figure 21. Removal of the bottom head from Capsule 1. Photos taken through the HFEF hot cell window.

3.3 Visual Examinations of Compacts

All Capsule 1 compacts were easily pushed out of the holder with little or no resistance, indicating sufficient clearance between the holder and the compacts to prevent binding. Initial photographs of all the compacts were taken through the hot cell window before the compacts were packaged into individual aluminum containers. These images are adequate to assess the presence of major surface degradation of the compacts but lack sufficient resolution for detailed inspection. Once a suitable stage can be constructed, some of the compacts will be photographed in greater detail using the visual examination machine (VEM) at HFEF. Figure 22 shows examples of the typical appearance of most compacts from Capsule 1 where there are no signs of degradation or abnormal coloring. However, some compacts from stacks 7, 8, 9, and 10 had some dark splotches and bright reflective specks. Figure 23 shows an example of some of the dark splotches and bright reflective specks that appeared on the surface of parts of some compacts from stacks 7–10. Inspection of these compacts with the VEM promises to provide much higher resolution images of these surface features.

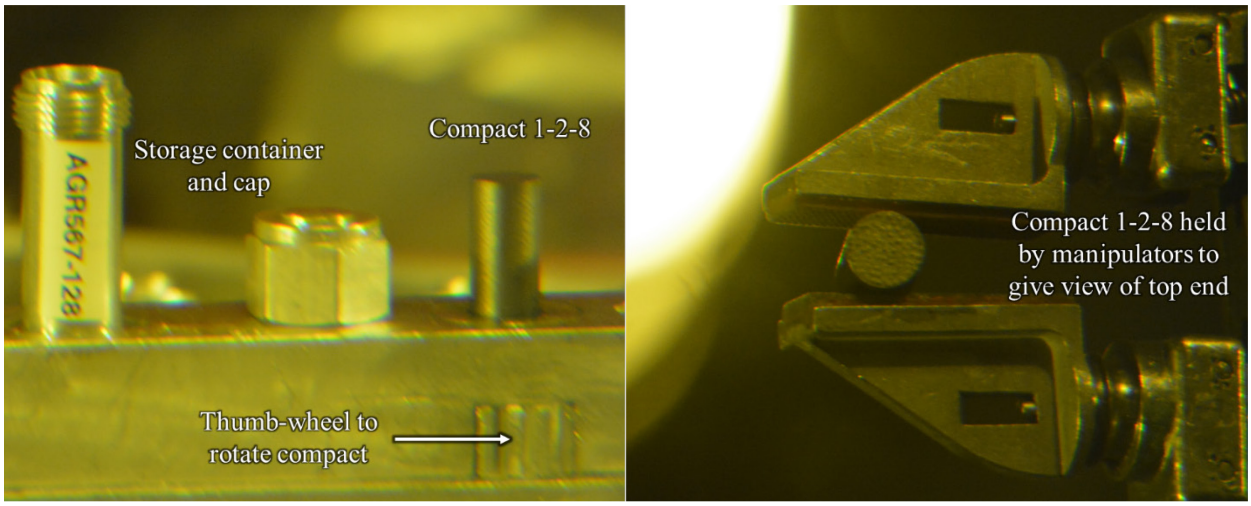

Figure 22. Photos of AGR-5/6/7 Compact 1-2-8 taken through the HFEF hot cell window.

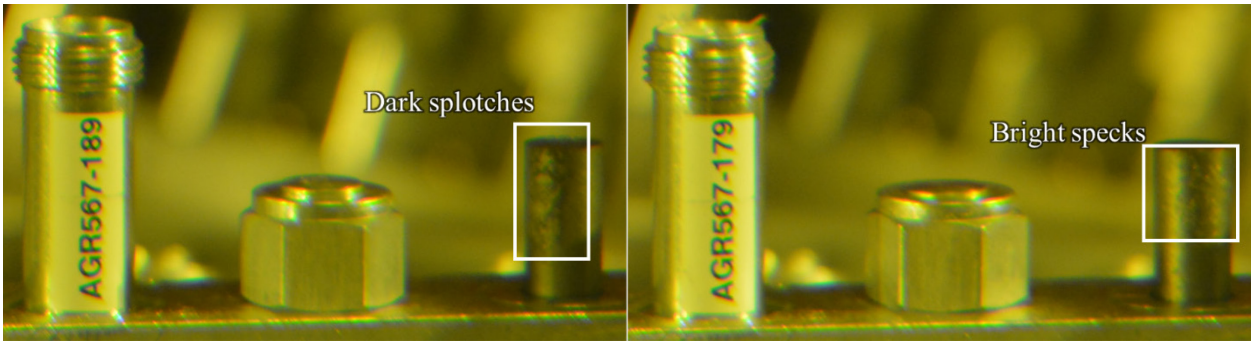

Figure 23. Dark splotches on one side of Compact 1-8-9 and bright reflective specks on one side of Compact 1-7-9.

3.4 Capsule 1 Holder Examination and Discovery of Deposits

The process of cutting the Capsule 1 stainless-steel shell left a burr at the top and bottom of the shell that prevented removal of the holder. A manual tool to ream and remove the burn was not effective; therefore, a tool that attached to the existing pipe cutter was devised and used successfully (see Figure 24a). With the burr removed, the Capsule 1 holder could be pushed out (see Figure 24b), and the interior of the shell could be examined (see Figure 24c). With the burr removed, the holder could be removed relatively easily, indicating sufficient clearance between the holder and the shell to prevent binding. The interior of the shell did not appear to have significant deposits or unusual coloring, and the shell will be leached to recover and fission products that may have deposited on its interior surface.

With the entire holder removed from the shell, a series of discrete deposits were observed on the outside of the holder. Figure 25 shows the three columns of deposits on the outside of the holder with surface discoloration adjacent to one deposit column also visible. Given the similar orientation and location compared to three distinct columns of deposits, it is possible this surface discoloration represents a nascent deposit similar to the others. The machined notch in the top of the holder is located between fuel stacks 10 and 1 and faced north during irradiation in ATR. Remnants of some of the TCs and/or gas inlet line extend a short distance above the top of the holder. It appears that TC-1-1, TC-1-2, and TC-1-3 were all pulled out of the holder during disassembly; however, the gas inlet line and all the other TCs are still in the holder.

Figure 3 shows the original location of all the TCs in the holder. TC-1-1 through TC-1-3 were located between fuel stacks 1, 2, and 3, respectively. A small piece of the webbing between stacks 2 and 3 broke off when the TC-1-2 was removed. The nubs machined around the outside of the holder are visible in some photos in Figure 25. There is some light-colored discoloration at the top of the holder with interspersed bright specks. There is a dark area toward the top of the holder aligned with stack 6. The three main columns of deposits appear dark with some bright interspersed specks. These main deposits appear to have thicknesses greater than the height of the machined nubs, which are 0.003 in. tall at the top of the holder. Photos of the holder suggest the deposits are thicker than the height of the nubs (see Figure 26). Other than the three main columns of deposits, some color variations, some minor scratches from disassembly, and a chip to the holder webbing between stacks 2 and 3, there are no indications of holder damage or irradiation-induced degradation.

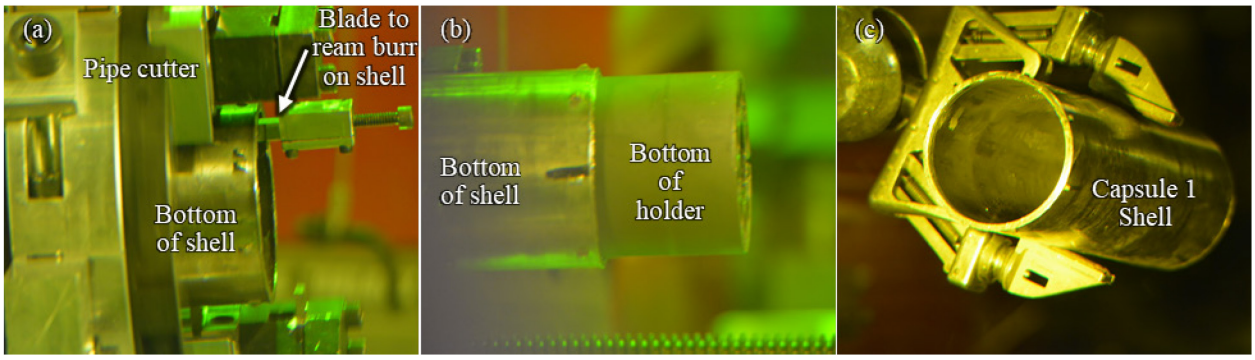

Figure 24. Blade attached to the pipe cutter drive to ream and remove the burr on the shell (a); Initial pushout of the Capsule 1 holder from the stainless-steel shell (b); partial interior view of the shell (c).

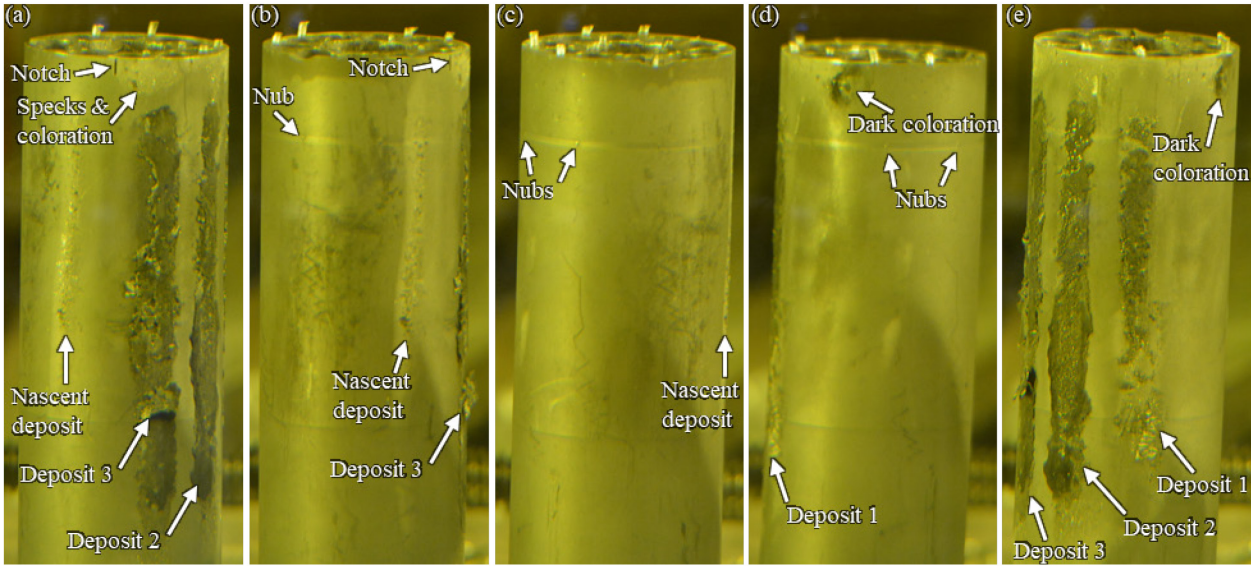

Figure 25. Series of photos of the Capsule 1 holder. Photos (b) through (e) were taken after rotating the holder counterclockwise.

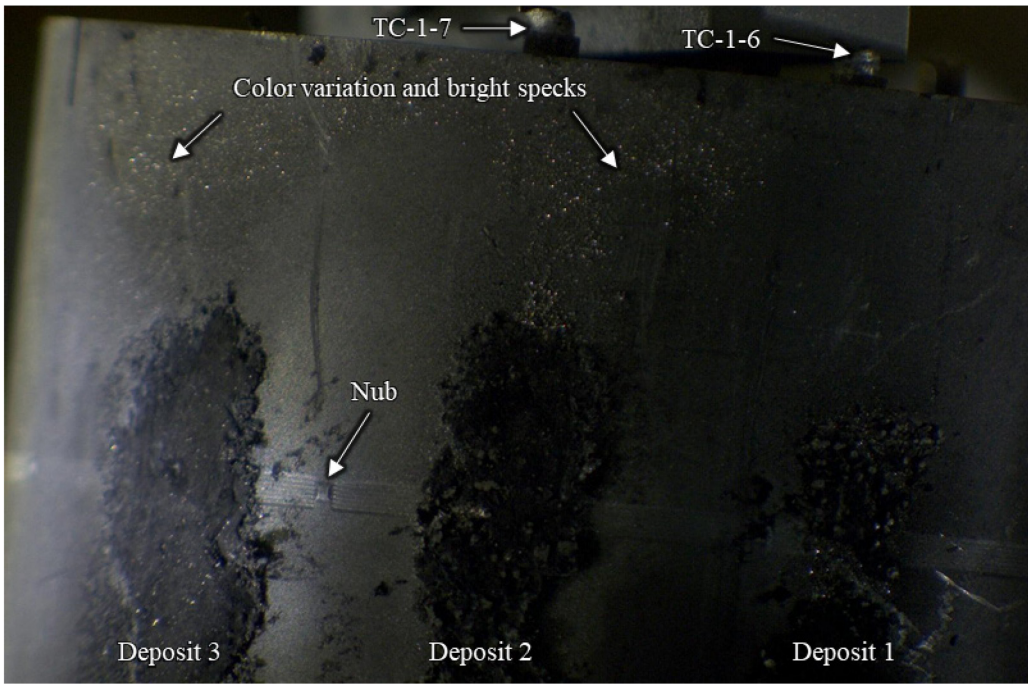

Figure 26. Photo of the top end of the Capsule 1 holder taken using the VEM.

The fuel channels and major deposits are labeled in Figure 27. Here, and in Figure 25e, it is apparent the deposits are aligned with the TC channels located between stacks of compacts. Deposit 1 is located along the instrument channel housing TC-1-6 between fuel stacks 7 and 8. Deposit 2 is located along TC-1-7 between fuel stacks 8 and 9. Deposit 3 is located along TC1-8 between fuel stacks 9 and 10. There was no instrumentation in between stacks 10 and 1, and there are no deposits in this region; however, there appears to be the beginning of a deposit on the outside of the holder along fuel stack 1. While higher resolution photos are needed, initial compact exams discussed in Section 3.3 showed potential variations in color (e.g., dark splotches and bright specks) in compacts from stacks 7–10.

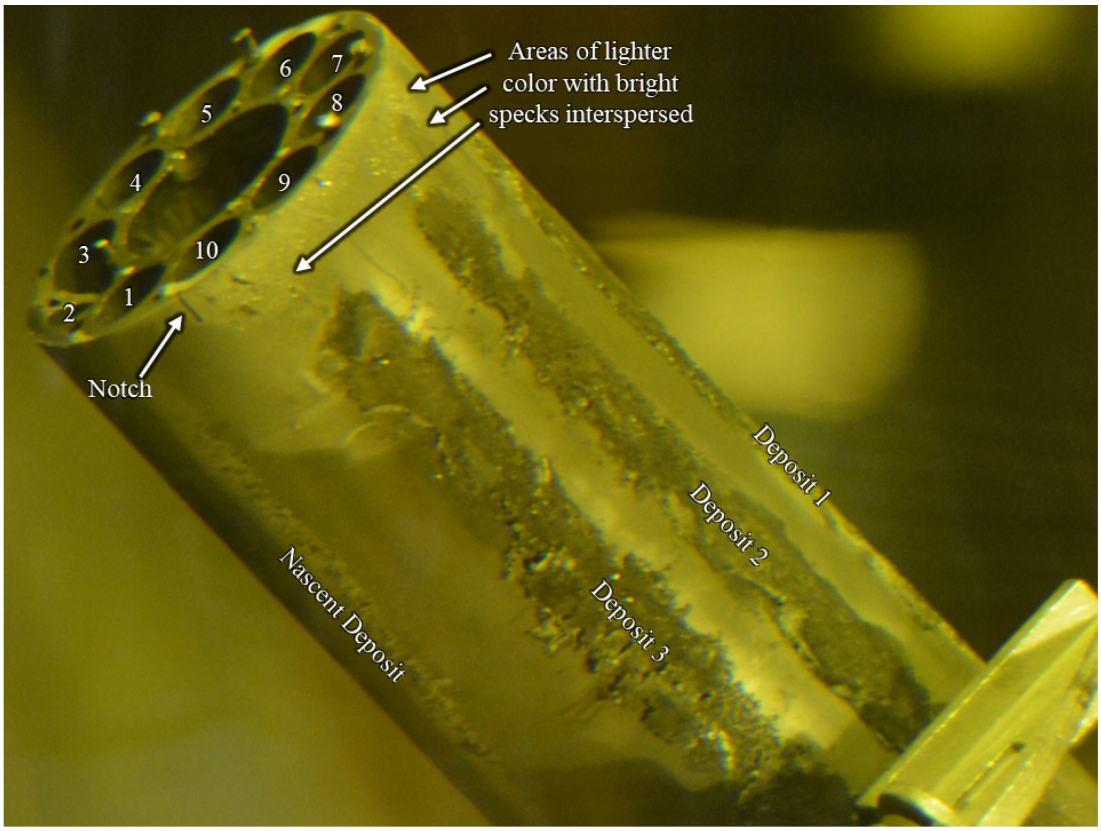

Figure 27. Photo of the holder showing the fuel stacks and major deposits.

A small portion of each of the three major columns of deposits was removed with tweezers, mounted on a microscopy stub, gamma counted at HFEF, and then transferred to the Irradiated Materials Characterization Laboratory for scanning electron microscopy (SEM) and elemental analysis via energy dispersive x-ray spectroscopy (EDS). Figure 28 shows a small flake of Deposit 3 being removed with tweezers and placed in a 0.5 in. diameter SEM stub. One stub was used for one sample from each of the three deposits. The three stubs were placed in an aluminum holder and counted together using the HFEF out-of-cell gamma station. The activities of gamma-emitting radioisotopes were decay-corrected to July 23, 2020, at 1:10 am Mountain Standard Time using the half-lives in the ENDF/B-VII.1 library (Chadwick et al. 2011). This date corresponds to the AGR-5/6/7 EOI plus one day. Using EOI+1d as a reference date has been the standard practice for referencing fission product inventories in AGR fuels.

Table 2 summarizes the decay-corrected activities measured in the samples taken of the deposits. The activities of measured gamma-emitting fission products were also compared to the calculated production of these fission products determined via physics simulations (Sterbentz 2020). In row 2 of Table 2, the decay-corrected activities were divided by the calculated inventories for all of Capsule 1 to give the fraction of the Capsule 1 inventory that was detected in the sampled deposits. The activities of key fission products in an average Capsule 1 fuel particle were calculated from values given in Sterbentz (2020). The measured activities shown in the first row of Table 2 were divided by the inventories calculated to have been produced in a single average Capsule 1 fuel particle to express the quantity of these fission products in terms of the number of average particle equivalents (row 3 of Table 2). For example, 58% of an average particle's inventory of Ag-110m was detected in the samples taken from the deposits.

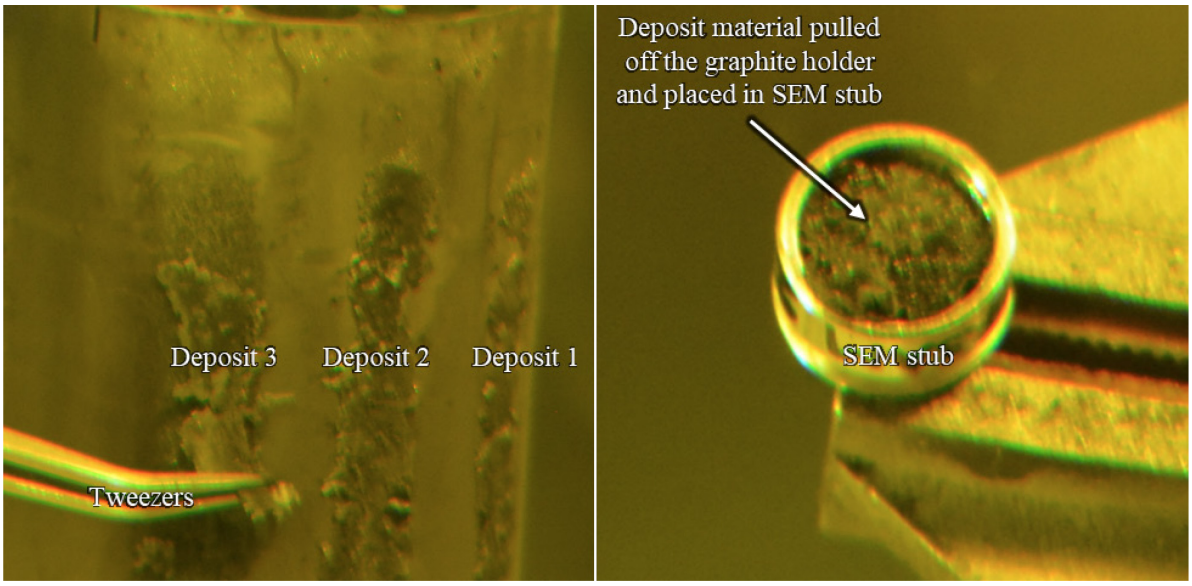

Figure 28. Sampling small portions of the deposits on the outside of the graphite holder and securing them in a SEM stub for gamma counting and analysis via SEM and EDS.

Table 2. Total inventory of gamma-emitting radioisotopes in the three sampled portions of the deposits on the Capsule 1 holder. All values are referenced to EOI+1.

	Co-58	Co-60	Ag-110m	Sb-125	Cs-134	Cs-137	Eu-154	Eu-155
Measured Activity at EOI+1 (μCi)	2.63E+3	3.57E+1	5.18E+0	1.83E+1	2.61E+2	2.36E+2	2.72E+1	1.41E+1
Fraction of Capsule 1 Inventory	N/A[a]		1.88E-6	6.82E-7	7.65E-7	6.40E-7	2.31E-6	1.72E-6
Number of Equivalent Average Capsule 1 Particles Worth	N/A[a]		5.81E-1	2.11E-1	2.37E-1	1.98E-1	7.14E-1	5.33E-1

a. Physics predictions were not made for Co-58 and Co-60 because they are not produced by fission in U or Pu.

Given the small amount of the deposited material sampled from the Capsule 1 holder and gamma counted, the quantities of gamma-emitting fission products measured in this material are substantial. Depending on the quantity of radiocesium measured outside of TRISO fuels (such as in the graphite holder), it can indicate a degraded SiC layer(s) in the fuel in the vicinity of where that radiocesium was detected (Hunn et al. 2016). The Cs-134 inventory in the sampled deposits is 0.24 particle equivalents, equivalent to a capsule fraction of 7.65E-7. For comparison, the Cs-134 inventory in the entire AGR-2 Capsule 2 graphite holder was 1.46 particle equivalents or a capsule fraction of 5.1E-5 (Stempien and Demkowicz 2020).

In addition to the gamma-emitting fission products, two activation products, Co-58 and Co-60 were prevalent in the sampled deposits. Co-60 may be produced from neutron activation of Fe, Ni, and Co. Production of the relatively short-lived nuclide Co-58 (half-life 70.8 d) is from neutron activation in Ni-58, the most abundant natural isotope of Ni. To put the amount of measured Co-60 and Co-58 into perspective, the Co-60 detected in the deposits sampled from AGR-5/6/7 can be compared to the Co-60 detected in the AGR-3/4 Capsule 8 outer ring. The AGR-5/6/7 graphite holders were made from IG-430, and the AGR-3/4 Capsule 8 outer ring was made from IG-110. IG-110 and IG-430 graphites have similar

specifications for impurities with nominal quantities of Fe, Co, and Ni of <0.01, < 0.05, and <0.1 ppmw, respectively.[b] In the AGR-3/4 Capsule 8 outer ring (which was 2 in. long with an inner diameter of about 1 in. and an outer diameter of about 1.5 in.), neutron activation of trace impurities in this ring during the AGR-3/4 irradiation resulted in 1.1 μCi of Co-60 at EOI + 1 (Harp, Stempien, and Demkowicz 2021). In the small portions of the AGR-5/6/7 Capsule 1 holder deposits that were sampled, the Co-60 activity is 35.7 μCi. Assuming the three small samples of the deposits that were collected and measured were each about 1 cm long, 1 cm wide, and 0.013 cm (0.005 in.) thick, their combined volume would be about 800 times less than the volume of the AGR-3/4 Capsule 8 outer ring. This means the Co-60 concentration ($\mu Ci/cm^3$) in the sampled deposits from AGR-5/6/7 Capsule 1 is about 26,000 times higher than it was in the AGR-3/4 Capsule 8 outer ring. Thus, the amount of Co-60 in the AGR-5/6/7 Capsule 1 deposits is much higher than the amount of Co-60 that would be expected from simple neutron activation of trace impurities in the IG-430 graphite used in the Capsule 1 holder. One possible source of the Co activation products is Ni that originated from the Cambridge Type N TCs. Elemental analysis of the deposits with SEM/EDS will be used to confirm the presence and concentration of Ni.

3.5 Preliminary Metrology of the Compacts and Graphite Holder

Basic preliminary results from metrology of the Capsule 1 holder and fuel compacts will be briefly summarized in this section. A detailed report on the disassembly and metrology of all the AGR-5/6/7 capsules will be produced in the future. All the Capsule 1 compacts were subjected to measurements for length and diameter, and these dimensions measured in PIE were compared to the dimensions determined during pre-irradiation characterization. The inner diameters of the Capsule 1 graphite holder fuel stacks were measured and compared to their pre-irradiation dimensions. The compact lengths were measured using a micrometer. The compact diameters were measured at three axial locations (top, middle, and bottom) at two azimuths per location. The diameters of the fuel stack channels in the graphite holder were measured at four axial locations (top, top middle, bottom middle, and bottom) at two azimuths.

Except for Compact 1-1-1 (which registered a length increase of 0.1%) all compacts decreased in length by amounts ranging from 0.1 to 1.8%, with an average length decrease of 0.94 ± 0.29%. The compacts all decreased in diameter by 0.6 to 1.8%, with an average diameter decrease of 1.2 ± 0.32%. The extent of length and diameter change in the fuel compacts is consistent with observations from AGR-1 and AGR-2 (Demkowicz et al. 2015; Stempien et al. 2021). Compacts with higher fast neutron fluences saw more diameter reduction than compacts with lower neutron fluences with no signs of turn-around (i.e., no signs of less diameter reduction beyond a certain threshold in neutron fluence).

After irradiation, the diameters of the fuel stack channels in the graphite holder were all similarly larger than in the as-fabricated condition. The diameters increased by 0.58–0.62%. For comparison, the standard deviations in the measured, as-fabricated diameters were 0.07–0.12%, indicating that the small diameter increases indicated by PIE metrology are genuine. Given that the compacts could be easily pushed out of the graphite holder, the compact diameters shrank, and the graphite holder fuel stack inner diameters increased, there does not seem to have ever been a point at which the compact-holder gap was reduced to zero during irradiation.

[b] These values come from unpublished elemental analyses from the Advanced Graphite Creep program. An article by Lee, Ghosh, and Loyalka (2018) reports impurities for IG-110 only.

4. ISSUES WITH CAPSULE DESIGN

4.1 Heightened Concern of Ni Attack on TRISO SiC Considered at AGR-5/6/7 Final Design Review

Initial AGR-5/6/7 PIE has observed deposits on the outside of the Capsule 1 graphite holder that align with the TC channels machined into the holder, in between adjacent stacks of fuel compacts. Sampling of these deposits and measurements made via gamma spectrometry suggest that Ni is a major constituent of the deposits. Preliminary visual exams of the compacts that came from locations adjacent to the deposits suggests some discoloration and even reflective specks on the compact surfaces.

First row transition metals Cr, Mn, Fe, Co, Ni are known to react with SiC, and these reactions can be deleterious to the structural integrity of the SiC layer of TRISO-coated particles. PIE results from the AGR-2 experiment indicated that a few particles experienced SiC failure due to Ni attack (Hunn et al. 2018; Stempien et al. 2021). A possible source of Ni in AGR-2 was the Type N TCs located in very close proximity (within approximately 1.5 mm) of the fuel. The assumption is that one or more of the Nb sheaths developed a crack which allowed nickel to migrate from the TCs.

AGR-1 also used Type N TCs with Nb sheaths; however, AGR-2 Capsule 2 had a higher operating temperature than AGR-1 and it is likely that this led to a higher rate of metal diffusion compared to AGR-1. It is also possible that there were no cracks in the Nb sleeves in the Type N TCs used in AGR-1. The AGR-1 experiment included Inconel-sheathed TCs, surrounded by Nb protective sleeves that were located about 1.5 mm from the fuel compacts. These TCs experienced temperatures of approximately 900–1050°C and there were no signs of Ni attack of SiC in the fuel particles. This was a known successful configuration, and it was assumed that it could be copied for TCs measuring temperatures in this range in the AGR-5/6/7 test.

Unlike AGR-2, the Type N TCs in AGR-5/6/7 had nickel sheaths surrounded with Nb protective sleeves (see Section 1.2.2), i.e., a much larger quantity of Ni in contact with substantial Nb. Figure 29 shows a calculated Nb-Ni binary phase diagram, with a eutectic point at 1184°C. While this temperature would represent an obvious upper limit to be avoided, past studies of Nb-Ni diffusion couples also showed extensive diffusion at temperatures as low as 1100°C, with diffusion zones exceeding 1 mm after 24 h at this temperature (Birks and Seebold 1961). It was therefore important not to place TCs with this configuration at temperatures above 1100°C. As a result of concerns raised at the AGR-5/6/7 final design review about Ni attack of SiC, changes were made to the design requirements, as summarized in Table 3. Initial projections of TC temperatures in the outer positions of the Capsule 1 holder were <1050°C, even at a worst-case power level of 20 MW (Figure 30). This circumstance corresponds to row 4 in the “New Requirements” where Ni may be placed in the capsule provided it is operating temperature is less than 1050°C and surrounded by a Mo or Nb sleeve (Table 3).

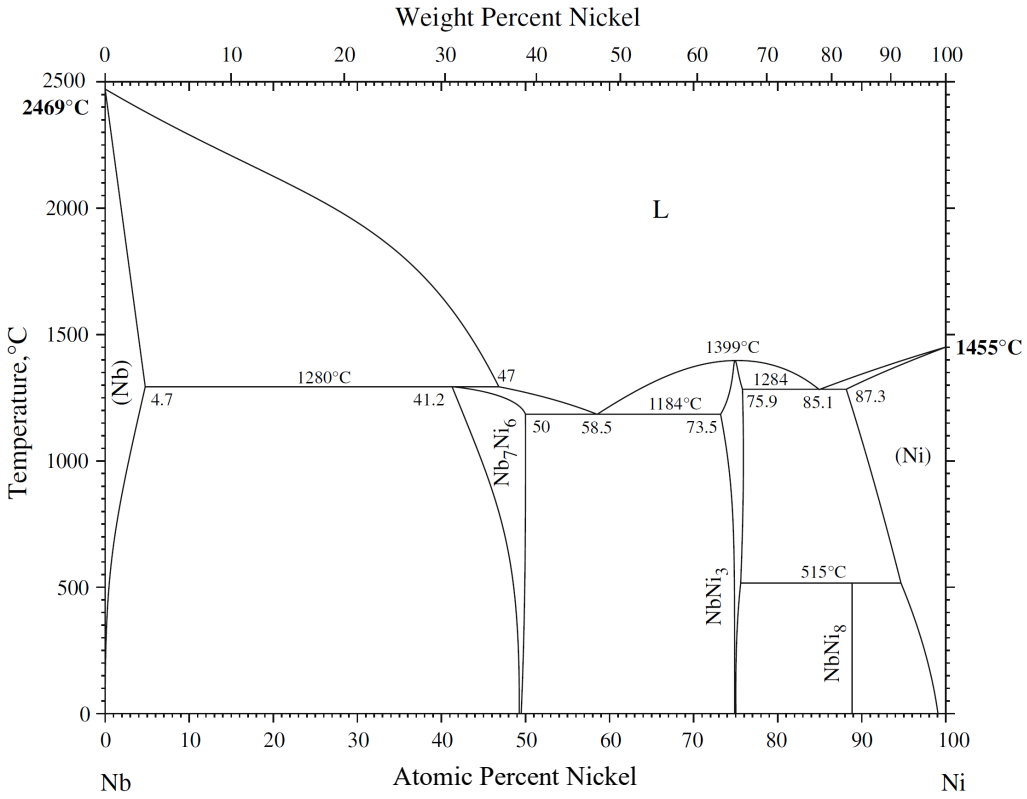

Figure 29. Nb-Ni binary phase diagram calculated by Okamoto (2008).

Table 3. Summary of changes in the AGR-5/6/7 design requirements intended to eliminate the possibility of Ni attack of SiC.

Metals in Capsules – Original Requirements

Temperature	Distance from Fuel Compact	Acceptable Materials
Not specified	>4 mm	Ni and other transition elements can be used without sleeves
Not specified	<4 mm	Ni surrounded by Mo sleeve, or Nb sleeve; or Mo, Nb alone

Metals in Capsules – New Requirements

Temperature	Distance from Fuel Compact	Acceptable Materials
>1050 °C	>4 mm	Ni* surrounded by crack-resistant Mo sleeve, or program-approved high-temperature ceramic sleeve; or Mo, Nb
>1050 °C	<4 mm	Ni bearing materials are not permitted; only Mo, Nb, and ceramics (e.g. TC insulation) are permitted
<1050 °C	>4 mm	Ni surrounded by Mo or Nb sleeves (it is not necessary to demonstrate crack resistance of Mo sleeve for these lower temperatures); or Mo, Nb
<1050 °C	<4 mm	Ni surrounded by crack-resistant Mo sleeve, or Nb sleeve, or program-approved high-temperature ceramic sleeve; or Mo, Nb

4.2 As-run Calculated Temperatures Exceeded those from Pre-test Predictions

Figure 30 shows the pre-test predicted temperatures in AGR-5/6/7 Capsule 1. The temperatures from this analysis were used to make the design decision that Cambridge Type N TCs with Ni sheaths and Nb sleeves could be used in the outer positions of the Capsule 1 holder while adhering to the New-Requirements criteria identified in Table 3 during the design review. Figure 31 is an update of the temperature profile in Capsule 1 made after the first cycle of irradiation. Temperatures in red are calculated temperatures, while those in black are measured temperatures. If, at the time of the design review, the pre-test calculated temperatures were similar to these as-run temperatures, then Type N TCs would not have been allowed in these locations because the calculated temperatures were above 1050°C. This circumstance would have corresponded to row 2 in the New-Requirements table.

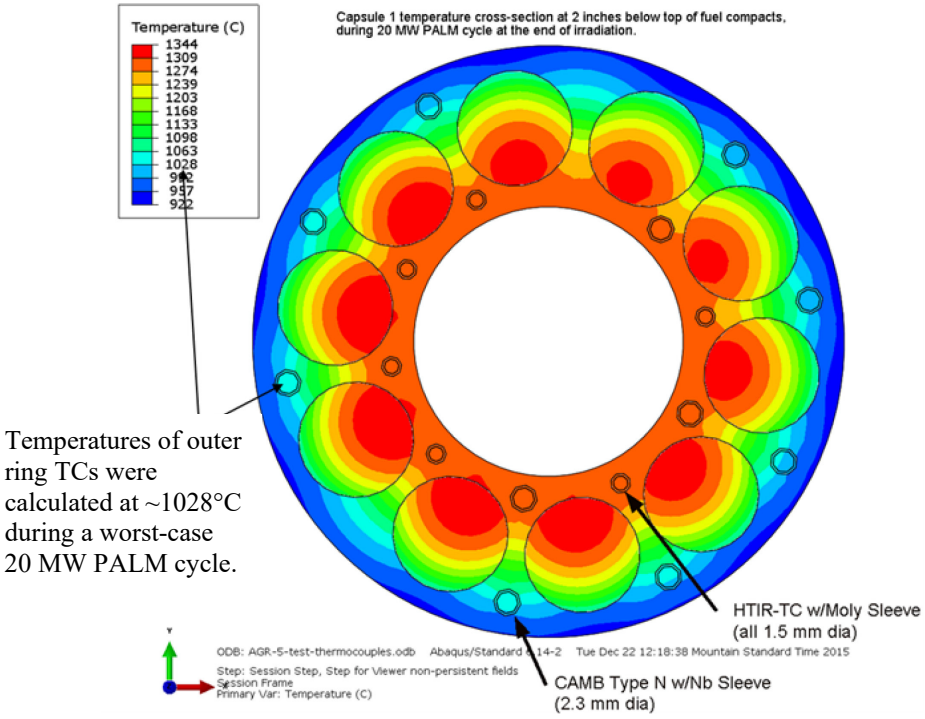

Figure 30. Pre-irradiation temperature projections in AGR-5/6/7 Capsule 1.

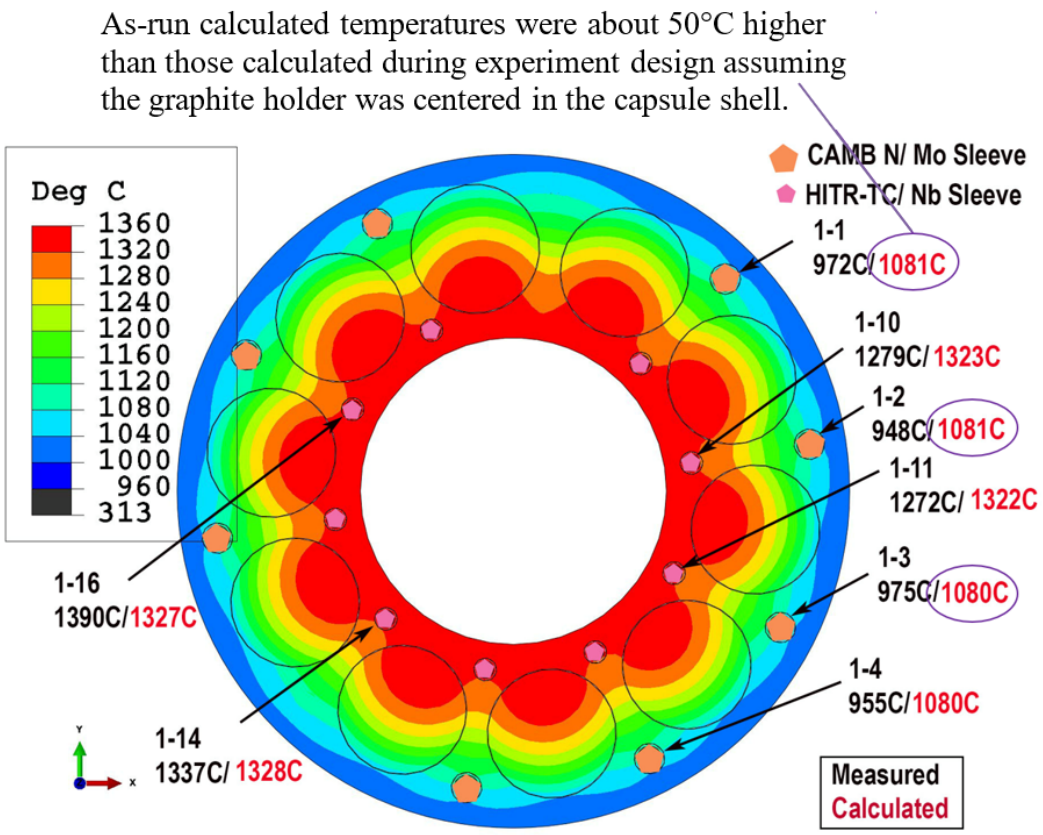

Figure 31. Temperatures calculated in the Capsule 1 holder after the first AGR-5/6/7 irradiation cycle compared to measured temperatures.

4.3 Design Error Resulted in Loose Fit Between Holder and Capsule Shell

Temperatures in the capsules were controlled by a gas gap between the graphite fuel holder and the capsule shell that was immersed in the ATR primary coolant water. Small standoffs (often referred to as nubs) were machined into the fuel holder outer surface to center the holder in the capsule shell while still allowing for the necessary temperature control gap. As shown on the left in Figure 32, these standoffs should have had a close fit to the capsule shell inside diameter but, due to a design error, the nubs were too short and the Capsule 1 holder was loose in the Capsule 1 shell. Figure 33 shows excerpts from two different sheets within the same drawing package where the outer diameter of the nubs was unintentionally smaller than the inner diameter of the stainless-steel shell. This allowed the holder to shift inside the capsule shell by as much as 0.005 in. and produce a gas gap large on one side and small on the other (see right side of Figure 32).

The design was conceptualized as shown here with the nubs essentially touching the capsule shell inner diameter.

Due to failure to verify this aspect of the drawing, the nubs were too small.

This was the likely offset during irradiation—with the holder offset to the southeast.

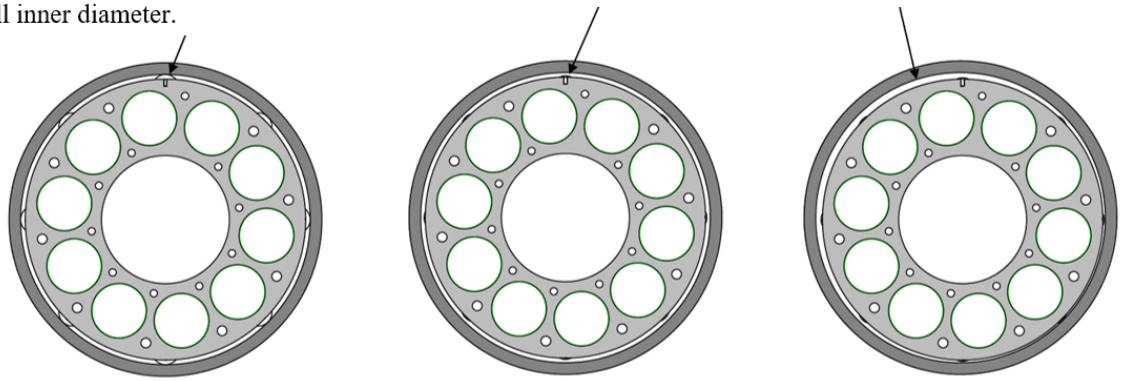

Figure 32. Depiction of the intended gas gap between the graphite holder and the stainless-steel capsule shell and a potential offset whereby the holder was not centered in the shell.[c]

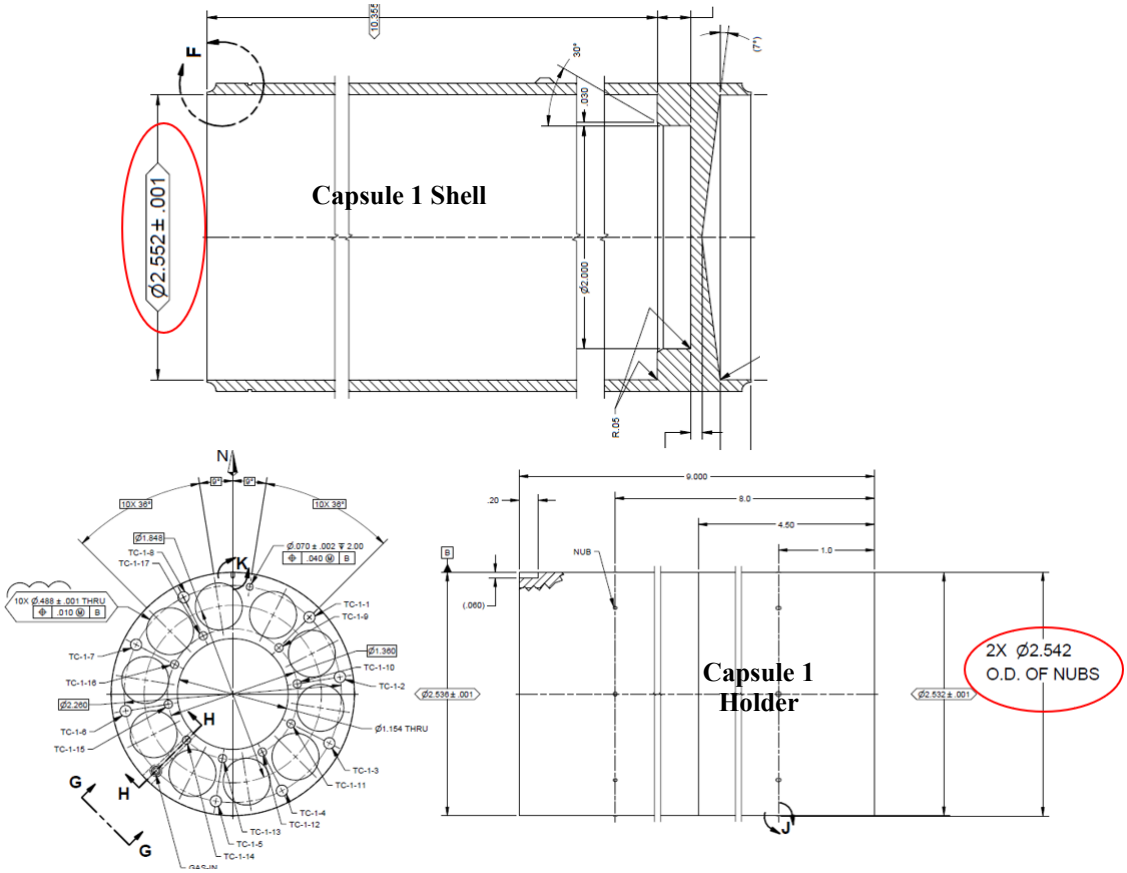

Figure 33. Excerpts from DWG 604661 sheets 5 and 6 showing how the outer diameter of the holder nubs should have been the same as the inner diameter of the Capsule 1 shell.

[c] The gas gap shown in these illustrations has been increased by a factor of five to make the offset more visible. The design gas gap was 0.008 in. between the outer diameter of the holder and the inner diameter of the stainless-steel capsule shell (the thickness of two sheets of paper). The intention was that there be no clearance between the nubs' outer diameters and the shell inner diameter; however, the nubs were built too small.

Figure 34 was produced as part of the thermal analysis performed for the AGR-5/6/7 experiment before significant PIE had begun (Pham et al. 2021). At left in Figure 34 is the temperature contour for the Capsule 1 graphite holder if it were centered in the stainless-steel capsule shell. The figure at right in Figure 34 is the result of shifting the holder northeast (toward the top right in this contour) by 0.001 in. with respect to the shell, which results in a rise in temperature in the southwest (bottom left in this contour). The temperature rise is on the order of 40–50°C. Because of the design error discussed above, the holder in Capsule 1 could have shifted as much as 0.005 in. The evidence available indicates the shift was actually to the south/southeast, which would have produced high temperatures in the northwest quadrant near fuel stacks 7–10 (near outer-ring TCs TC-1-6, TC-1-7, and TC-1-8 and inner-ring TCs TC-1-15, TC-1-16, and TC-1-17). Such a change in holder orientation within the capsule would result in fuel temperatures significantly different than those determined by the current thermal analysis. A thermal analysis of fuel temperatures with varying degrees of holder radial offsets beyond 0.001 in. is currently being pursued.

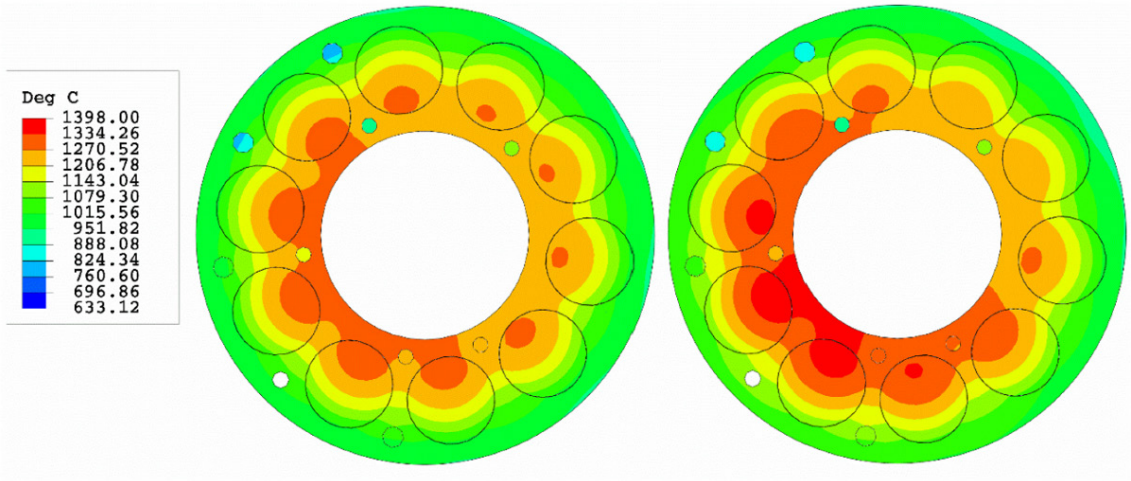

Figure 34. Comparison of temperature contours in the Capsule 1 holder with the holder centered (left) and with a 0.001 in. offset to the northwest (right).

The drawing error shown in Figure 33 was present in all five capsules in AGR-5/6/7, i.e., there was the same 0.010 in. diametrical clearance between the outer diameter of the standoffs and the inner diameter of the capsule shell (allowing a 0.005 in. radial shift). However, some important considerations are listed below.

1. All capsules except Capsule 1 have through-tubes that pass through the body of the fuel holders. These tubes form a sort of cage, which in addition to the standoffs, provide a redundant centering feature. By comparison, Capsule 1 had only TC leads and one gas line penetrating the capsule top head and into the graphite holder, which allowed some degree of movement of the graphite holder relative to the capsule top head.
2. Capsules 2, 4, and 5 ran at considerably lower temperatures than Capsule 1. Capsule 3 had temperatures higher than Capsule 1, and it did have Type N TCs in hot regions, however these TCs had ceramic (ZrO_2) protective sleeves surrounding them, and the TCs were more than 4 mm from the fuel.[d]

[d] There is some evidence that Capsule 3 experienced a few particle failures (see Table 15 of Pham et al. 2021). It is possible that these failures were also a result of Ni attack. Due to extremely high temperatures in Capsule 3, some Ni atoms may have migrated through the ceramic protective sleeves by solid state diffusion and made their way to the fuel particles even though they were more than 4 mm away.

3. With the exception of Capsule 2, the other capsules had larger gas gaps which would reduce the strength of the effect of a possible 0.005 in. offset.

4.4 Capsule 1 Temperature Data During Irradiation

Figure 35 illustrates measured and calculated temperatures from Capsule 1 about two weeks into the first irradiation cycle. Note that the measured temperatures (black font) for the outer ring of TCs are very consistent at <1000°C. This did not raise any concerns at the time. Figure 36 shows the trends of all the Cambridge Type N TCs in the outer positions in the Capsule 1 holder. Nothing in these data caused concern during irradiation.

Upon further consideration, TCs 1-7 and 1-8 are very deep in the fuel holder (meaning they extend from the top of the holder to within 1 in. of the bottom of the 9 in. long holder), and as a result, the thermal junctions at their tips near the bottom of the holder should have been cooler than the other TCs. This is indeed what is shown by the associated calculated and measured values in Figure 35 and Figure 36. However, the upper portions of these TC wires toward the middle of the capsule would have seen hotter temperatures than those at their thermal junctions and these temperatures would not have been detected. Figure 37 shows that the junction of TC-1-8 was not far from the bottom of the fuel holder (a relatively cool location), but the upper part of this TC could have been experiencing temperatures above 1200°C (above the Ni-Nb eutectic melting point) if the holder was shifted southeast as is suspected.

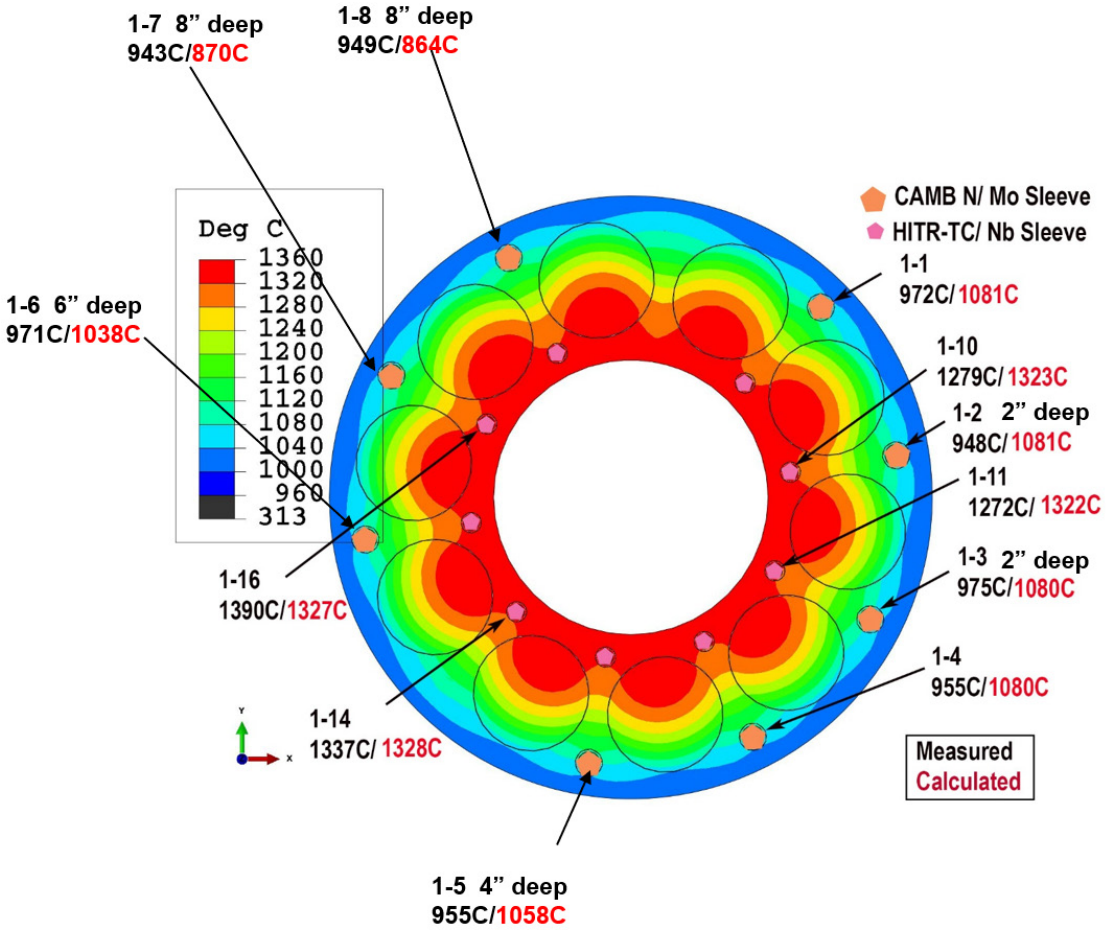

Figure 35. Calculated versus measured thermocouple temperatures two weeks from the start of irradiation.

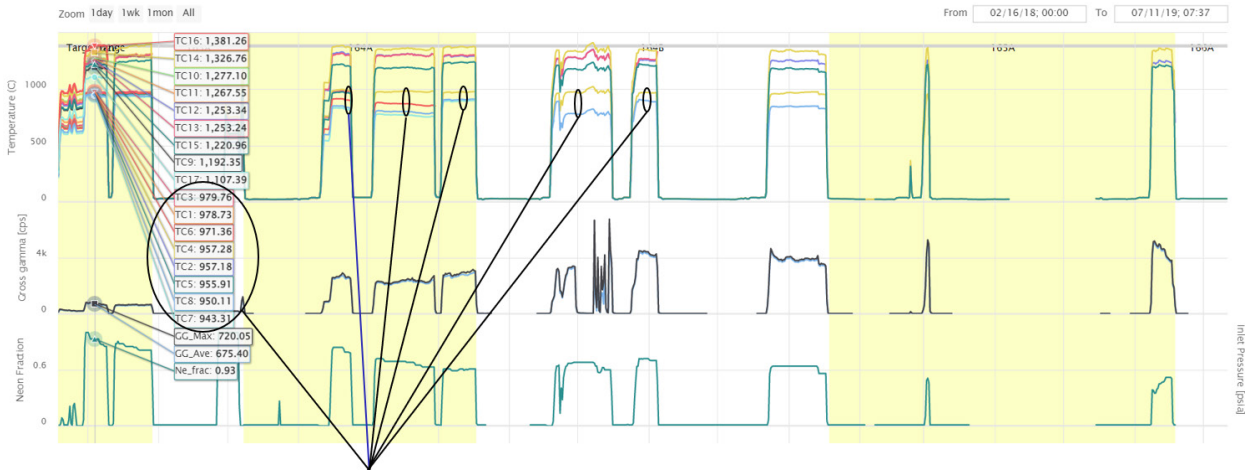

Figure 36. Temperature trends in Capsule 1 during irradiation from 2/16/2018 to 7/11/2019. The outer-ring TCs (TC-1-1 through TC-1-8) are highlighted to show they were always below 1000°C.

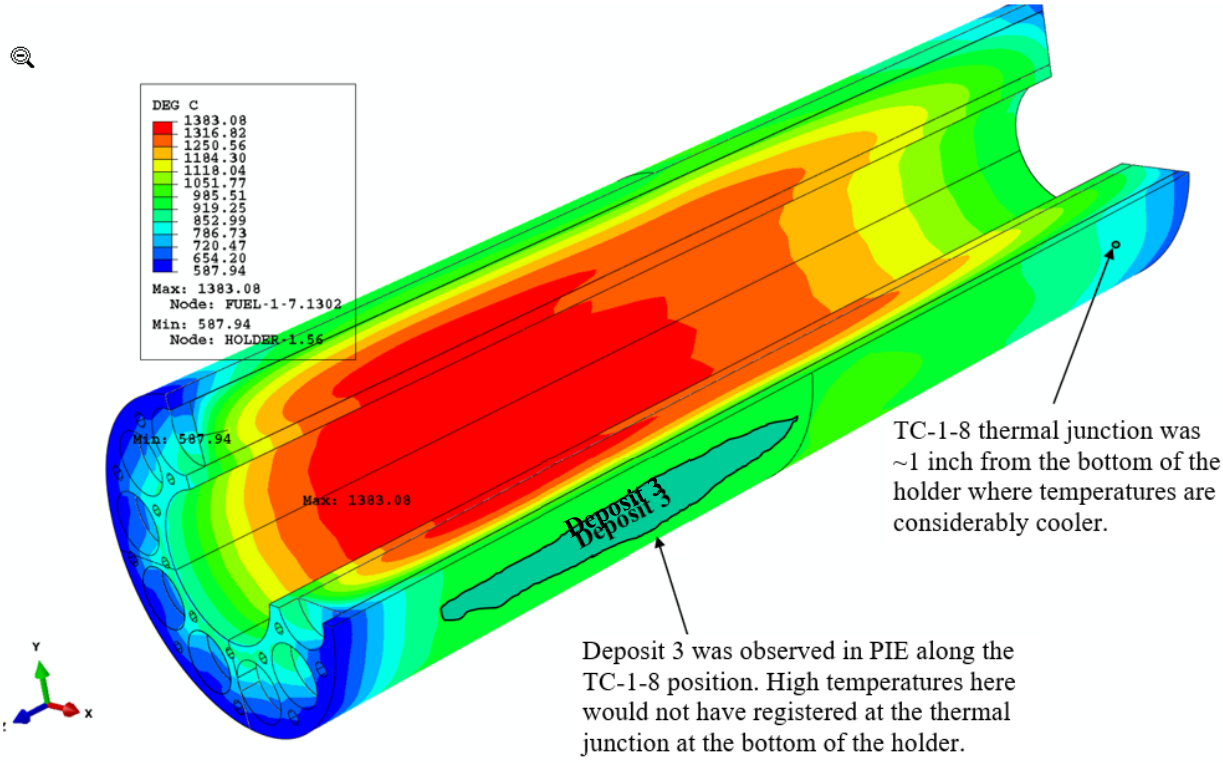

Figure 37. Temperature contours for the Capsule 1 graphite holder. The TC-1-8 thermal junction is near the bottom of the fuel holder (about 1 in. from the bottom); thus, the suspected high temperatures further up the wire would have gone unmeasured. Similar events would have affected TC-1-6 and TC-1-7.

4.5 Contributing Factors

The loose fit between the graphite fuel holder and capsule shell and the resulting radial displacement of the holder relative to the shell is likely the predominant factor that could have contributed to higher-than-expected temperatures in the Ni-sheathed Cambridge Type N TCs (e.g., TC-1-6 through TC-1-8) in the north and northwest positions in Capsule 1, but other factors may have contributed.

A point of note is that fuel failures were not evident in Capsule 1 until the latter half of irradiation, during the end of Cycle 166A. Figure 38 shows the temperature measured in TC-1-14, the GG counts in the FPMS, the neon gas fraction, and the gas flow rate from near the beginning of Cycle 166A in July to its end in October. The entire ATR power history is also shown, and the portion of that history corresponding to Cycle 166A has been highlighted.

Before the start of Cycle 166A, the thermal model clearly indicated that the desired particle temperature distribution was not being achieved. In response, the setpoint of TC-1-14 (an inner-ring, ZrO_2 sleeved HTIR TC located between stacks 6 and 7) was increased 70°C on July 28, 2019, during the early stage of Cycle 166A. This change was accomplished by increasing the neon fraction in the gas. After this temperature increase was implemented, TC-1-14 was reading at a temperature of about 1385°C, but the model predicted its temperature should have been about 80°C lower. Subsequent furnace testing of TCs of the same configuration as TC-1-14 indicate they experience substantial negative drift (50–100°C) when exposed to temperatures above 1350°C. Therefore, it was likely that TC-1-14 had experienced negative drift and was at a temperature well over 1400°C when it failed on September 6, 2019, during a reactor scram.

Additional temperature increases were implemented after TC-1-14 failed in an effort to increase the overall fuel particle temperature distribution. Figure 38 shows a number of increases in the neon fraction after the first increase on July 28, 2019. The GG counts increased after the associated temperature increases, as expected when fuel temperature increases, but distinct particle failures were not observed until flow was restarted on September 30, 2019. The relatively rapid onset of significant failure (evidenced by a rapid increase in fission gas activity in the FPMS) suggests that the mechanism of coating degradation was not significant until sometime in Cycle 166A, and this could have been related to these further increases in capsule temperature. These temperature increases were made even though the team was aware that the thermal model could be underpredicting fuel temperatures. This was done because of the assumption there was considerable margin in what the particles could withstand compared to the experiment goals of achieving 10% of the particles above 1350°C. Because all the Ni-sheathed, Nb-sleeved Cambridge Type N TCs had run below 1000°C before they failed, the possibility of overheating these TCs was not part of the decision process.

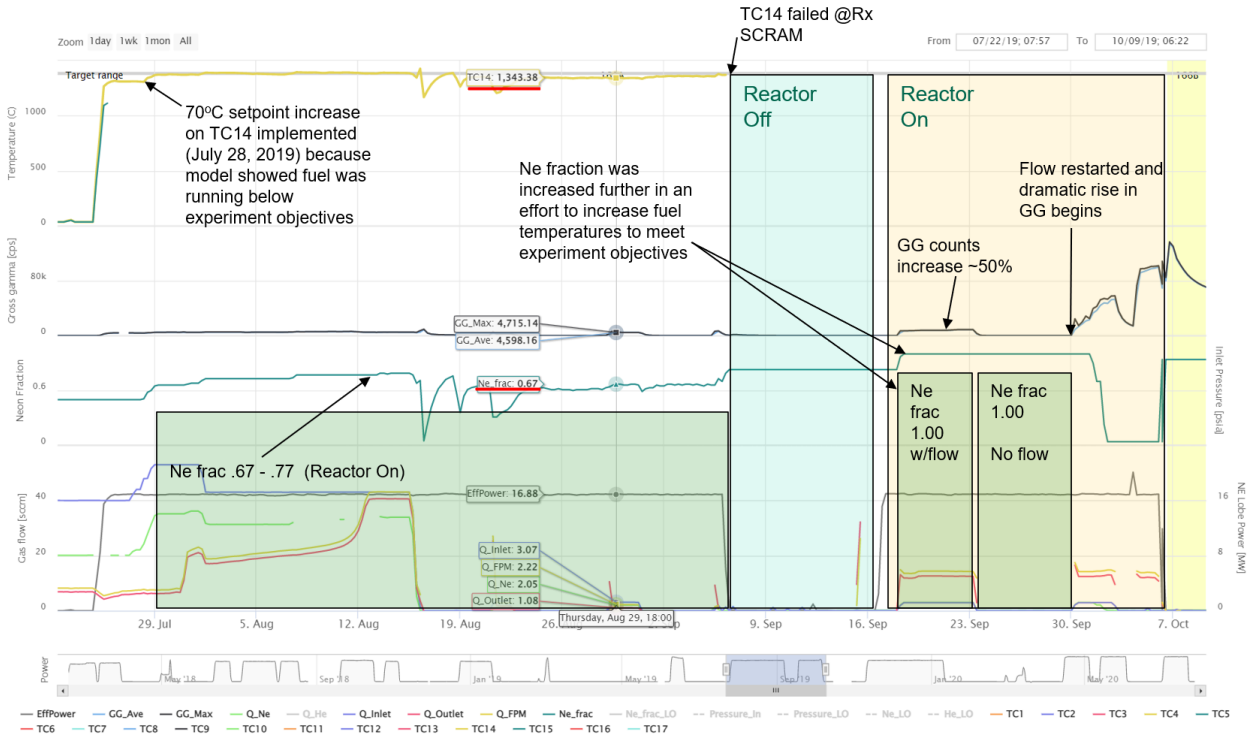

Figure 38. Capsule 1 data from July 22, 2019, to the end of Cycle 166A.

5. CONCLUSIONS AND FUTURE WORK

5.1 Summary and Conclusions

Online measurements of fission gas release from Capsule 1 indicated significant rates of TRISO fuel particle failure that were much higher than expected. Some temperature measurements available at the time were somewhat hotter than predicted by the thermal model. Until PIE could start, it was not clear if the apparent fuel failures were related to non-fuel components in the test train or if the failures were inherent to the fuel that was shown to be of acceptable quality in pre-irradiation characterization. Now that PIE of Capsule 1 components and fuel has begun and the fuel compacts and graphite fuel holder have undergone some initial non-destructive examinations, it appears likely that the cause of the fuel failure was precipitated by errors in the capsule design and not by subpar performance of the fuel itself.

When the Capsule 1 holder was removed from the stainless-steel Capsule 1 shell, three columns of well-defined deposits were visible along the TC channels between fuel stacks 7, 8, 9, and 10, and what appeared to be the beginning of a fourth column of deposit was observed near Stack 1. The locations of the three main columns of deposits coincided with the three longest Ni-sheathed, Nb-sleeved, Cambridge Type N TCs (i.e., TC-1-6, TC-1-7, and TC-1-8) and were generally located in the axial portion of the holder that had the highest temperatures. The apparent thickness of these deposits exceeds the height of the nubs machined into the compact holder, suggesting the holder was not centered in the shell and that the gas gap on the side of the holder with these deposits was larger than the gas gap on the opposite side of the holder, leading to higher temperatures in the northwest region of the capsule. Some portions of these deposits appeared to have bright, reflective specks in them. Compacts recovered from the fuel stacks adjacent to these deposits (i.e., stacks 7–10) had dark splotches and bright reflective specks not seen on compacts from other stacks. It is hypothesized that overheating of these TCs resulted in the transport of Ni to the holder (forming deposits on its surface), to the fuel causing some visual variations on the compacts' surfaces, and a chemical reaction between the Ni and the SiC to form Ni-silicides leading ultimately to widespread fuel failure in Capsule 1.

In addition to the observations made in PIE, several details of the capsule design, irradiation history, thermal analyses, and knowledge collected from prior AGR experiments also support the hypothesis that overheating of the TCs allowed Ni to escape the TCs and degrade the fuel, leading to its failure. The pre-test thermal predictions showed that the TCs placed in the outer ring would be at temperatures <1050°C during what was considered a worst-case scenario during a high-powered PALM cycle. Based on those predictions, Type N TCs with a Ni sheath and a Nb sleeve were used in the ring of TCs placed in channels near the outside of the holder. Early in the irradiation, it was found that the temperatures calculated by using actual ATR run data as input were about 50°C higher than those predicted in the pre-test thermal analyses, and if these temperatures were known at the time of the test train design, Ni-bearing TCs would not have been used in those positions.

To exacerbate the fact that the as-run calculated temperatures at the TC positions were higher than predicted, an error in the drawing of the graphite holder meant the nubs, relied upon to center the holder in the capsule shell, were smaller than intended and would allow an offset of up to 0.005 in., with a corresponding increase in the size of the gas gap. Thus, the true temperatures in a part of the capsule with the larger gas gap caused by the capsule being off-center could be even hotter than calculated in the as-run thermal analysis. The long TCs used near fuel stacks 7-10 extended through the hottest part of the capsule where it is estimated their temperatures could have been in excess of 1200°C; however, since the thermal junctions of these TCs were toward the bottom of the capsule where temperatures are much cooler, these high temperatures would not have been measured. The Ni-Nb binary phase diagram shows there is a eutectic that melts at 1184°C, and diffusion studies showed considerable Nb-Ni interdiffusion at 1100°C. Localized eutectic melting of the TC sheath and sleeve or extensive diffusion of Ni into the sleeve could have allowed Ni to escape and transport within the capsule. A few particles in AGR-2 Capsule 2 were found to have SiC failures from small amounts of Ni (presumably from a nearby TC that failed during irradiation) that reacted to form Ni-silicides. Thus, degradation of TRISO particles by Ni originating from TCs has precedence in AGR experiments, and the amount of Ni present in the AGR-5/6/7 Capsule 1 graphite holder appears to be much more extensive than observed in AGR-2.

5.2 Future Work

This document serves as a status report on the state of knowledge surrounding Capsule 1 as of April 2022. As of this writing, the available data suggest that the primary cause of fuel failure in AGR-5/6/7 Capsule 1 was thermal degradation of TCs which allowed Ni to become mobile in the capsule and cause damage to the SiC layer of numerous particles. Additional data are needed to verify this failure mechanism. Work currently in progress and planned for this year and beyond is intended to observe the fuel and other related components (such as the graphite holder) to obtain further data.

While gamma spectroscopy of the samples collected from the deposits on the graphite holder show Co-58 and Co-60 (transmutation products from the neutron activation of Ni), these samples will be undergoing elemental analysis in fiscal year 2022 to look specifically for Ni. Nickel attack in AGR-2 was confirmed via a complex process of deconsolidating suspect compacts, identifying individual particles with Cs loss by gamma counting, non-destructive examination of the identified particles to locate regions of SiC degradation, and cross sectioning and microscopy of the particles to examine the particles in detail.

For fiscal year 2022, deconsolidation-leach-burn-leach is planned for at least two Capsule 1 compacts followed by X-ray computed tomography of four selected particles to look for signs of coating degradation. Cross sectioning and microscopy of three Capsule 1 compacts will be conducted to look for signs of degraded particles. Initial visual exams of Capsule 1 compacts were performed via photographs taken through the hot cell window. Pending the construction of a suitable stage, compacts will be further examined using the VEM at HFEF.

In the following year, many particles will be mounted, polished, and subjected to electron microscopy and potentially other advanced microscopic techniques. After non-destructive examinations of the Capsule 1 holder (including gamma tomography) have been completed, the holder can be cross sectioned to look for signs of Ni dispersal in the holder. Improved thermal modeling to better establish the temperatures possible with a holder offset on the order of 0.005 in. or more are being pursued. Two competing effects, thermal expansion and irradiation induced shrinkage of the graphite holder, will also be considered for their effects on the size of the gas gap and the potential offset of the holder within the capsule shell. While results from these various analyses may be published in separate reports as they become available, a final report will be produced describing the cause of Capsule 1 fuel failure once all data are available.

6. REFERENCES

Birks, L.S. and R.E. Seebold. 1961. "Diffusion of Nb with Cr, Fe, Ni, Mo and stainless steel." *Journal of Nuclear Materials* 3:249–259. doi: 10.1016/0022-3115(61)90192-1.

Chadwick, M. B., M. Herman, P. Oblozinsky, et al. 2011. "ENDF/B-VII.1 Nuclear Data for Science and Technology: Cross-Sections, Covariances, Fission Product Yields and Decay Data." *Nuclear Data Sheets* 112: 2887–2996. doi: 10.1016/j.nds.2011.11.002.

Collin, B. P. 2018, "AGR-5/6/7 Irradiation Experiment Test Plan." PLN-5245, INL/MIS-17-43095, Rev. 1. Idaho National Laboratory.

Demkowicz, P. A., J. D. Hunn, R. N. Morris, I. van Rooyen, T. Gerczak, J. M. Harp, and S. A. Ploger. 2015. "AGR-1 Post Irradiation Examination Final Report." INL/EXT-15-36407. Idaho National Laboratory. doi: 10.2172/1236801.

Demkowicz, P., L. Cole, S. Ploger, and P. Winston. 2011. "AGR-1 Irradiated Test Train Preliminary Inspection and Disassembly First Look." INL/EXT-10-20722. Idaho National Laboratory. doi: 10.2172/1009153.

DWG 604660. 2015. "ATR Advanced Gas Reactor (AGR-5/6/7) Capsules 1 Thru 5 Assembly Weldment." Rev. 3. Idaho National Laboratory.

DWG 604661. 2015. "ATR Advanced Gas Reactor (AGR-5/6/7) Capsule 1 Assembly and Details." Rev. 5. Idaho National Laboratory.

Harp, J. M., J. D. Stempien, and P. A. Demkowicz. 2021. "Gamma Spectrometry Examination of the AGR-3/4 Irradiation." INL/EXT-20-58254, Rev. 1. Idaho National Laboratory. doi: 10.2172/1844232.

Hawkes, G. L. 2022. "AGR-5/6/7 Daily As-Run Thermal Analyses." ECAR-5633. Idaho National Laboratory.

Hunn, J. D., C. A. Baldwin, F. C. Montgomery, T. J. Gerczak, R. N. Morris, G. W. Helmreich, P. A. Demkowicz, J. M. Harp, and J. D. Stempien. 2018. "Initial Examination of Fuel Compacts and TRISO Particles from the US AGR-2 Irradiation Test." *Nuclear Engineering and Design* 329:89–101. doi: 10.1016/j.nucengdes.2017.09.017.

Hunn, J. D., C. A. Baldwin, T. J. Gerczak, F. C. Montgomery, R. N. Morris, M. C. Silva, P. A. Demkowicz, J. M. Harp, S. A. Ploger, I. van Rooyen, and K. E. Wright. 2016. "Detection and analysis of particles with failed SiC in AGR-1 fuel compacts." *Nuclear Engineering and Design* 306:36–46. doi: 10.1016/j.nucengdes.2015.12.011.

INL. 2021. "Technical Program Plan for INL Advanced Reactor Technologies Advanced Gas Reactor Fuel Development and Qualification Program." PLN-3636, INL/MIS-10-20662, Rev. 10. Idaho National Laboratory.

Lee, J. J., T. K. Gohsh, and S. K. Loyalka. 2018. "Comparison of NBG-18, NBG-17, IG-110 and IG-11 oxidation kinetics in air." *Journal of Nuclear Materials* 500: 64–71. doi: 10.1016/j.jnucmat.2017.11.053.

Marshall, D. W. 2017. "AGR-5/6/7 Fuel Specification." SPC-1352, Rev. 8, Idaho National Laboratory.

Nelson M. M., 2020. "AGR-5/6/7 Gas System – Analysis of Various Anomalies Encountered During Irradiation." ECAR-5114, Rev. 0, Idaho National Laboratory.

Okamoto, H. 2008. "Nb-Ni (Niobium-Nickel)." *Journal of Phase Equilibria and Diffusion* 29:210. doi: 10.1007/s11669-008-9277-0.

Pham, B. T., J. J. Palmer, D. W. Marshall, J. W. Sterbentz, G. L. Hawkes, and D. M. Scates. 2021. "AGR-5/6/7 Irradiation Test Final As-Run Report." INL/EXT-21/64221. Idaho National Laboratory.

Ploger, S., P. Demkowicz, and J. Harp. 2015. "AGR-2 Irradiated Test Train Preliminary Inspection and Disassembly First Look." INL/EXT-15-34997. Idaho National Laboratory. doi: 10.2172/1194020.

Scates, D. M., 2021. "Release-to-Birth Ratios for AGR-5/6/7 Operating Cycles 162B through 168A." ECAR-5352, Rev. 0, Idaho National Laboratory.

Stempien, J. D., J. D. Hunn, R. N. Morris, T. J. Gerczak, and P. A. Demkowicz. 2021. "AGR-2 TRISO Fuel Post-Irradiation Examination Final Report." INL/EXT-21-64279. Idaho National Laboratory.

Stempien, J. D. 2020. "AGR-5/6/7 Post-Irradiation Examination Plan." PLN-6110. INL/EXT-20-59111. Idaho National Laboratory.

Stempien, J. D. and P. A. Demkowicz. 2020. "AGR-2 Irradiation Experiment Fission Product Mass Balance." INL/EXT-19-53559, Rev. 1. Idaho National Laboratory.

Stempien, J. D., F. J. Rice, P. L. Winston, and J. M. Harp. 2016. "AGR-3/4 Irradiation Test Train Disassembly and Component Metrology First Look." INL/EXT-16-38005, Rev. 1. Idaho National Laboratory.

Sterbentz, J. W. 2020. "JMOCUP Physics Depletion Calculations for the As-Run AGR-5/6/7 TRISO Particle Experiment in ATR Northeast Flux Trap." ECAR-5321, Rev. 0. Idaho National Laboratory.

Appendix A

Capsule 1 Compact Time-Averaged Temperature, Burnup, and Fast Neutron Fluence at the End of Irradiation

The low fission powers during the two low-power PALM cycles (Cycle 163A and 167A) led to significantly lower fuel temperatures in all capsules. Therefore, the time-average temperature calculations were performed for two scenarios: the first one included all days of irradiation and the second one excluded two low-power PALM cycles. The time-average fuel temperatures in Table 4 for both scenarios, and Capsule 1 neon fractions during Cycle 168A were zero.

Table 4. Compact time-averaged temperature, burnup, and fast neutron fluence at the end of irradiation.

Compact	Time-Averaged Minimum Temperature (°C)	Time-Averaged Volume-Averaged Temperature (°C)	Time-Averaged Peak Temperature (°C)	Burnup (% FIMA)	Fast Neutron Fluence (10^{25} n/m^2, E >0.18MeV)
1-1-1	588	762	882	5.78	1.62
1-2-1	737	884	993	7.34	2.07
1-3-1	810	967	1075	8.11	2.48
1-4-1	863	1027	1131	8.68	2.85
1-5-1	878	1053	1152	9.17	3.19
1-6-1	878	1065	1179	9.61	3.49
1-7-1	893	1091	1205	10	3.76
1-8-1	886	1094	1207	10.43	4
1-9-1	611	951	1163	11.09	4.17
1-1-2	588	761	881	5.66	1.62
1-2-2	736	883	991	7.35	2.07
1-3-2	810	966	1073	8.11	2.48
1-4-2	862	1026	1129	8.69	2.84
1-5-2	878	1052	1149	9.19	3.18
1-6-2	877	1064	1177	9.61	3.49
1-7-2	892	1090	1206	10.01	3.76
1-8-2	886	1096	1208	10.44	4
1-9-2	612	953	1165	11.12	4.16
1-1-3	592	765	885	5.86	1.64
1-2-3	739	887	996	7.42	2.11
1-3-3	812	969	1077	8.15	2.52
1-4-3	865	1029	1132	8.73	2.89

Compact	Time-Averaged Minimum Temperature (°C)	Time-Averaged Volume-Averaged Temperature (°C)	Time-Averaged Peak Temperature (°C)	Burnup (% FIMA)	Fast Neutron Fluence (10^{25} n/m^2, E >0.18MeV)
1-5-3	880	1055	1153	9.21	3.23
1-6-3	879	1067	1181	9.63	3.54
1-7-3	894	1094	1210	10.02	3.82
1-8-3	889	1100	1213	10.49	4.06
1-9-3	613	956	1169	11.22	4.22
1-1-4	594	772	893	6.13	1.69
1-2-4	745	894	1004	7.56	2.16
1-3-4	818	977	1086	8.26	2.58
1-4-4	871	1036	1140	8.8	2.96
1-5-4	884	1061	1160	9.27	3.3
1-6-4	884	1073	1188	9.68	3.62
1-7-4	899	1100	1217	10.12	3.9
1-8-4	893	1106	1219	10.59	4.14
1-9-4	617	961	1175	11.33	4.31
1-1-5	602	779	903	6.47	1.73
1-2-5	752	903	1014	7.71	2.21
1-3-5	826	987	1096	8.4	2.63
1-4-5	878	1046	1150	8.95	3.02
1-5-5	891	1070	1170	9.36	3.37
1-6-5	891	1083	1198	9.79	3.68
1-7-5	905	1109	1225	10.19	3.97
1-8-5	898	1112	1227	10.75	4.21
1-9-5	618	966	1182	11.53	4.38
1-1-6	603	785	910	6.63	1.75
1-2-6	757	911	1023	7.84	2.23
1-3-6	831	995	1105	8.5	2.65
1-4-6	884	1054	1159	9.05	3.04
1-5-6	896	1078	1178	9.46	3.39
1-6-6	896	1090	1204	9.88	3.7
1-7-6	911	1115	1229	10.36	3.99
1-8-6	902	1116	1231	10.89	4.23
1-9-6	622	969	1185	11.68	4.4
1-1-7	604	786	911	6.67	1.75
1-2-7	758	912	1024	7.85	2.23
1-3-7	833	997	1108	8.5	2.66

Compact	Time-Averaged Minimum Temperature (°C)	Time-Averaged Volume-Averaged Temperature (°C)	Time-Averaged Peak Temperature (°C)	Burnup (% FIMA)	Fast Neutron Fluence (10^{25} n/m^2, E >0.18MeV)
1-4-7	886	1057	1162	9.03	3.04
1-5-7	898	1081	1180	9.46	3.39
1-6-7	897	1091	1205	9.86	3.7
1-7-7	912	1115	1230	10.34	3.99
1-8-7	903	1116	1231	10.91	4.23
1-9-7	621	969	1185	11.67	4.4
1-1-8	603	781	906	6.42	1.73
1-2-8	754	907	1019	7.73	2.2
1-3-8	829	992	1103	8.4	2.63
1-4-8	882	1053	1158	8.95	3.02
1-5-8	895	1077	1177	9.38	3.36
1-6-8	895	1088	1203	9.78	3.68
1-7-8	908	1113	1227	10.22	3.97
1-8-8	899	1114	1229	10.76	4.21
1-9-8	620	967	1183	11.57	4.38
1-1-9	595	774	898	6.16	1.69
1-2-9	747	900	1011	7.58	2.16
1-3-9	822	984	1095	8.29	2.58
1-4-9	875	1045	1150	8.82	2.96
1-5-9	889	1070	1169	9.29	3.3
1-6-9	889	1082	1196	9.7	3.62
1-7-9	903	1106	1221	10.13	3.9
1-8-9	894	1107	1222	10.62	4.14
1-9-9	616	962	1176	11.4	4.31
1-1-10	593	767	889	5.89	1.65
1-2-10	741	890	1001	7.42	2.11
1-3-10	815	974	1084	8.17	2.52
1-4-10	868	1035	1139	8.74	2.89
1-5-10	883	1060	1160	9.23	3.24
1-6-10	883	1072	1187	9.64	3.55
1-7-10	897	1097	1211	10.04	3.82
1-8-10	889	1098	1212	10.49	4.06
1-9-10	614	955	1168	11.24	4.22
Average	**588**	**1001**	**1231**	**9.12**	**3.18**